Chapter 3

Distinguishing between Reaction Intermediates and Spectators: A Kinetic Study of Acetone Oxidation Using Ozone on a Silica-Supported Manganese Oxide Catalyst

3.1 Introduction

This chapter concentrates on the kinetics and mechanism of the catalytic oxidation reaction between acetone and ozone. The 10 wt. % MnO_x/SiO_2 catalyst will be used for this investigation since it was determined to be more active for the reaction than the 3 wt. % MnO_x/SiO_2 catalyst. A detailed kinetic study will be performed by varying acetone partial pressure, ozone partial pressure, and reaction temperature. Both acetone and ozone turnover frequencies (TOFs) will be calculated based on conversion, and they will be used to determine rate expressions and kinetic parameters for the acetone and ozone reaction. Both a power rate law and Langmuir-Hinshelwood model will be used in fitting the kinetic data. The Langmuir-Hinshelwood model will be developed from a proposed mechanism that will based on experimental evidence. Raman spectroscopy will be used to measure adsorbate coverages and temperature programmed desorption (TPD) measurements will be used to calibrate the Raman signals. Finally, steady-state coverages obtained from separate transient and steady-state experiments will be

compared to verify the role of the adsorbed intermediates in the proposed reaction mechanism.

3.2 Experimental Section

3.2.1 Materials

A 10 wt. % manganese oxide catalyst (using MnO_2 as the basis) was used for all experiments. The synthesis details are reported in Chapter 2, but briefly, the catalyst was prepared by incipient wetness impregnation of an aqueous solution of manganese acetate ($Mn(CH_3COO)_2 \cdot 4H_2O$, Aldrich, 99.99 %) on a SiO_2 support followed by drying and calcination at 773 K.

The gases used in this study included oxygen (Air Products, > 99.6 %) and helium (Air Products, > 99.6 %), which were passed through gas purifiers (Alltech, Model 4658) to eliminate moisture. Acetone (Burdick and Jackson, 99.9+ %) was used as received.

3.2.2 Spectroscopic and Kinetic Measurements

Laser Raman spectroscopy and kinetic data were obtained utilizing the combined reactor system (Fig. 2.1) previously described in Chapter 2. Briefly, the spectroscopic part of the system was made up of an argon ion laser (514.5 nm, Spex Lexel 95), a holographic notch filter (Kaiser, Super Notch Plus), a single stage monochromator (Spex, 500 M), and a CCD detector (Spex, Spectrum One). The powder catalyst sample (~ 0.2 g) was pressed (201 MPa) into a thin wafer of 1.5 cm diameter and 0.1 cm thickness and was held in place by a stainless steel cap at the end of a rotating ceramic rod. The sample

was enclosed by a synthetic quartz (Suprasil) cell provided with inlet and outlet ports to serve as an *in situ* reactor. The cell was wrapped in heating tape, and a thermocouple was placed in a well just 0.3 cm away from the catalyst sample to measure the temperature. The gas delivery part of the system included a two-stage bubbler used for the vaporization of liquid acetone. The Antoine equation [1] was used to obtain the acetone vapor pressure (9.25 kPa at 273 K), and the flow rate of helium (~6.8 μmol/s = 10 cm^3/min) was adjusted to give the desired gas-phase acetone concentration. Pure oxygen (120 μmol/s = 180 cm^3/min) was fed to an ozone generator (OREC, V5-0), which produced ozone via corona discharge, and the exit ozone concentration was measured with an ozone monitor (In USA, Model H1). A gas chromatograph (GC) (SRI, Model 8610C) equipped with flame ionization and thermal conductivity detectors was used for measuring acetone, CO, and CO_2 concentrations.

Prior to all measurements, the catalyst sample was pretreated at 723 K for 2 h in a mixture of oxygen and helium to remove excess moisture and carbonaceous impurities from the sample. A secondary helium flow (220 μmol/s = 320 cm^3/min) was added to make the total flow rate of the feed for all experiments (340 μmol/s = 500 cm^3/min) which was made up of 35 mol % oxygen and 65 mol % helium. The concentrations of acetone and ozone were varied for the experiments but were always ≤ 1.0 mol %.

Detailed kinetic measurements were performed for the oxidation reaction of acetone and ozone over the 10 wt. % MnO_x/SiO_2 catalyst. In one set of experiments, the inlet partial pressure of acetone was varied over the range of 101 Pa (1,000 ppm) to 405 Pa (4,000 ppm) while the inlet partial pressure of ozone was held constant at ~790 Pa (~7,800 ppm). In another set of experiments, the inlet partial pressure of ozone was

varied over the range of 101 Pa (1,000 ppm) to 1,013 Pa (10,000 ppm) while the inlet partial pressure of acetone was held constant at ~193 Pa (~1,900 ppm). These measurements were carried out at reaction temperatures of 318, 333, 353, and 373 K while monitoring both acetone and ozone consumption rates. Similar, blank kinetic experiments were also conducted for the reaction between acetone and ozone with no catalyst or support present in the reactor.

The Raman spectroscopy study (Chapter 2) that was carried out on the 10 wt. % MnO_x/SiO_2 catalyst identified two adsorbed species on the surface of the catalyst during the reaction between acetone and ozone. An acetone intermediate was found with a characteristic feature at 2930 cm^{-1} while a peroxide species attributed to ozone was found with a feature at 890 cm^{-1}. In this work steady-state Raman spectroscopy experiments were carried out on the 10 wt. % MnO_x/SiO_2 catalyst sample to measure the coverages of the adsorbed intermediates associated with acetone and ozone. These experiments utilized the same conditions as used for the kinetic experiments on the 10 wt. % catalyst sample except that only the lowest reaction temperature of 318 K was used.

Transient Raman spectroscopy experiments were also performed on the 10 wt. % catalyst sample at 318 K to measure the evolution of adsorbate coverage with respect to time. Acetone addition, acetone removal, ozone addition, and ozone removal experiments were conducted at initial acetone and ozone partial pressures of 193 and 793 Pa (1,900 and 7,800 ppm), respectively. In all cases the measurements began at steady-state (removal experiments) or ended at steady-state (addition experiments).

3.2.3 Temperature Programmed Desorption (TPD) Measurements

Integrated peak areas from the Raman spectroscopy measurements were calibrated by quantitative analysis of temperature program desorption (TPD) traces for acetone and ozone. The TPD measurements were conducted using a standard flow system equipped with a computer-interfaced mass spectrometer (Dycor / Ametek Model MA100). As for the kinetic and spectroscopic experiments, quantities of ~0.2 g of the catalyst were first pretreated at 723 K for 2 h in oxygen (35 mol %) and helium (65 mol %) at a total flow rate of 340 μmol/s (500 cm^3/min). For the ozone TPD experiments, ozone (1013 Pa = 10,000 ppm) was introduced to the reactor for 1 h at 298, 273, and 261 K. Low temperatures were used to obtain saturation coverage on the catalyst surface. After the initial 1 h treatment, the ozone was cut off, and helium was introduced to the sample at 68 μmol/s (100 cm^3/min). The sample was heated at 0.17 K/s (10 K/min) to 673 K while the desorption signal for O_2 (*m/e* = 32), the only desorption product, was monitored. The O_2 desorption peak was quantitated with pulses of pure oxygen from a calibrated dosing volume (19.6 μmol). For the acetone TPD experiments, acetone at a partial pressure of 811 Pa (8,000 ppm) was introduced to the reactor for 1.5 h at 298, 273, and 261 K to obtain saturation adsorption, and an identical procedure was used for the ozone experiment. A higher acetone partial pressure of 1216 Pa (12,000 ppm) was also used but yielded the same results. The acetone desorption signal was calibrated with an acetone pulse (1.05 μmol). The acetone TPD experiment was repeated at 273 K using a pure, calcined (6 h in air at 773 K) silica sample.

3.3 Results

3.3.1 Temperature Programmed Desorption (TPD) Measurements

Previous work done in our laboratory showed that ozone adsorbs on manganese oxide in the form of a peroxide species (O_2^{2-}) and then desorbs as molecular oxygen [2,3]. In the present investigation ozone TPD experiments allowed the determination of the saturation amount of the adsorbed peroxide intermediate on the surface of the 10 wt. % MnO_x/SiO_2 catalyst by measuring the desorption of molecular oxygen as a function of adsorption temperature. Similarly, acetone TPD experiments allowed determination of the saturation amount of the adsorbed acetone intermediate. For both the ozone and acetone TPD experiments, maximum adsorption was achieved at a treatment temperature of 273 K. Table 3.1 gives the results of the TPD measurements along with the surface area and molecular oxygen chemisorption results reported in Chapter 2. Both ozone and acetone TPD experiments gave well-defined desorption peaks at ~385 K for oxygen and ~345 K for acetone. The amount of peroxide species (derived from ozone) adsorbed on the catalyst surface was 14 μmol/g while the amount of acetone intermediate adsorbed on the catalyst surface was 550 μmol/g. The amount of atomic oxygen chemisorption was 98 μmol/g. Acetone TPD experiments done on the silica support gave an adsorption amount for acetone of 790 μmol/g at a desorption temperature of ~350 K.

Table 3.1. Acetone and ozone surface area, molecular oxygen uptake, and TPD values for 10 wt. % MnO_x/SiO_2 and pure SiO_2.

Sample	SA $m^2\ g^{-1}$	O_2 Uptake $\mu mol\ g^{-1}$	Ozone TPD $\mu mol\ g^{-1}$	Ozone TPD $\mu mol\ m^{-2}$	Acetone TPD $\mu mol\ g^{-1}$	Acetone TPD $\mu mol\ m^{-2}$
10 wt. % MnO_x/SiO_2	210	49	14	0.067	550	2.6
SiO_2	320	0	0	0	790	2.5

3.3.2 Steady-State Raman Spectroscopy Measurements

Steady-state, *in situ* Raman spectroscopy experiments conducted on pure silica and the 10 wt. % MnO_x/SiO_2 catalyst at 298 K are shown in Figure 3.1. These experiments were conducted as described earlier with a total flow rate of 340 μmol/s (500 cm^3/min) and concentrations of oxygen and helium being roughly 35 mol % and 65 mol %, respectively. The feature at 280 cm^{-1} due to a Si-O vibration was used as an internal standard so that a reasonable comparison could be made between different experiments on the 10 wt. % MnO_x/SiO_2 catalyst, as well as measurements on pure silica. Figure 3.1a) displays the Raman spectrum for the 10 wt. % MnO_x/SiO_2 catalyst when acetone was included in the gas mixture at a concentration of 0.2 mol % and Figure 3.1b) the spectrum when the concentration was doubled to 0.4 mol %. The increase in acetone concentration led to a slight increase in peak intensity and area of the band attributed to the adsorbed acetone intermediate (2930 cm^{-1}). Figure 3.1c) shows a Raman spectrum for pure silica with acetone at a concentration of 0.2 mol %, and Figure 3.1d) shows the spectrum when the concentration of acetone was doubled to 0.4 mol %. Again, the increase in acetone concentration lead to an increase in peak intensity and area for the Raman band associated with the adsorbed acetone intermediate (2930 cm^{-1}). Overall the intensities on the SiO_2 were much higher than on the catalyst.

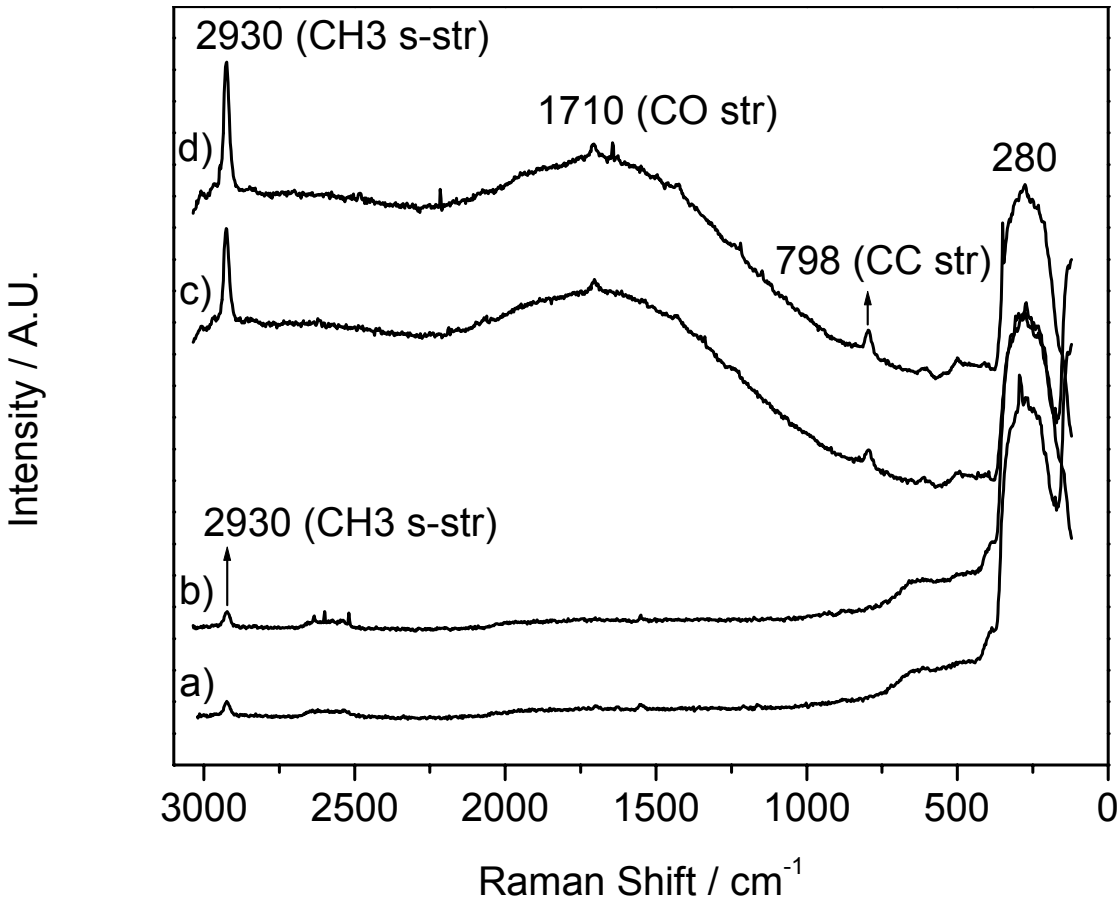

Figure 3.1. Steady-state, *in situ* Raman spectroscopy results (298 K) for the a) 10 wt. % MnO_x/SiO_2 sample in acetone flow (0.2 mol %), b) 10 wt. % MnO_x/SiO_2 sample in acetone flow (0.4 mol %), c) pure SiO_2 in acetone flow (0.2 mol %), and d) pure SiO_2 in acetone flow (0.4 mol %).

Steady-state, *in situ* Raman spectroscopy experiments were also conducted on the 10 wt. % MnO_x/SiO_2 catalyst at 318 K utilizing the same varying partial pressure conditions as were used in the kinetic experiments. Figure 3.2 shows the Raman spectra when the initial acetone partial pressure was varied (93 – 394 Pa), and the initial ozone partial pressure was kept constant (790 Pa). Figure 3.3 shows the Raman spectra when the initial ozone partial pressure was varied (274 – 1097 Pa), and the initial acetone partial pressure remained constant (193 Pa).

Using the Raman spectra presented in Figures 3.2 and 3.3, surface coverage values were calculated at 318 K for the two adsorbed intermediates at the different reactant partial pressure conditions. The surface coverage for the acetone intermediate, θ_A, was calculated by integrating the Raman peak at 2930 cm^{-1} and dividing the resulting peak area by the area obtained when acetone alone was saturated on the surface of the catalyst. Likewise, the surface coverage for the peroxide intermediate, θ_{O2*}, was determined by integrating the Raman peak at 890 cm^{-1} and dividing that peak area by the area obtained when the peroxide species was saturated on the catalyst surface. The saturated surface concentration of acetone (~811 Pa, 273 K) was 2.6 $\mu mol/m^2$ and resulted in a Raman peak area for the 2930 cm^{-1} band of 2040 while the saturated surface concentration of the peroxide species (~1013 Pa, 273 K) was 0.067 $\mu mol/m^2$ and resulted in a peak area for the 890 cm^{-1} band of 11,700 (Table 3.1). At 318 K when the reacting mixtures contained an acetone partial pressure of 394 Pa and an ozone partial pressure of 790 Pa, the resulting peak areas for the 2930 cm^{-1} and 890 cm^{-1} bands were 1090 and 1150, respectively. These values corresponded to surface acetone and peroxide concentrations of 1.4 $\mu mol/m^2$ and 0.0066 $\mu mol/m^2$, respectively and coverages for

acetone, θ_A, and peroxide, θ_{O2*}, intermediates equal to 0.53 and 0.098, respectively (Fig 3.4).

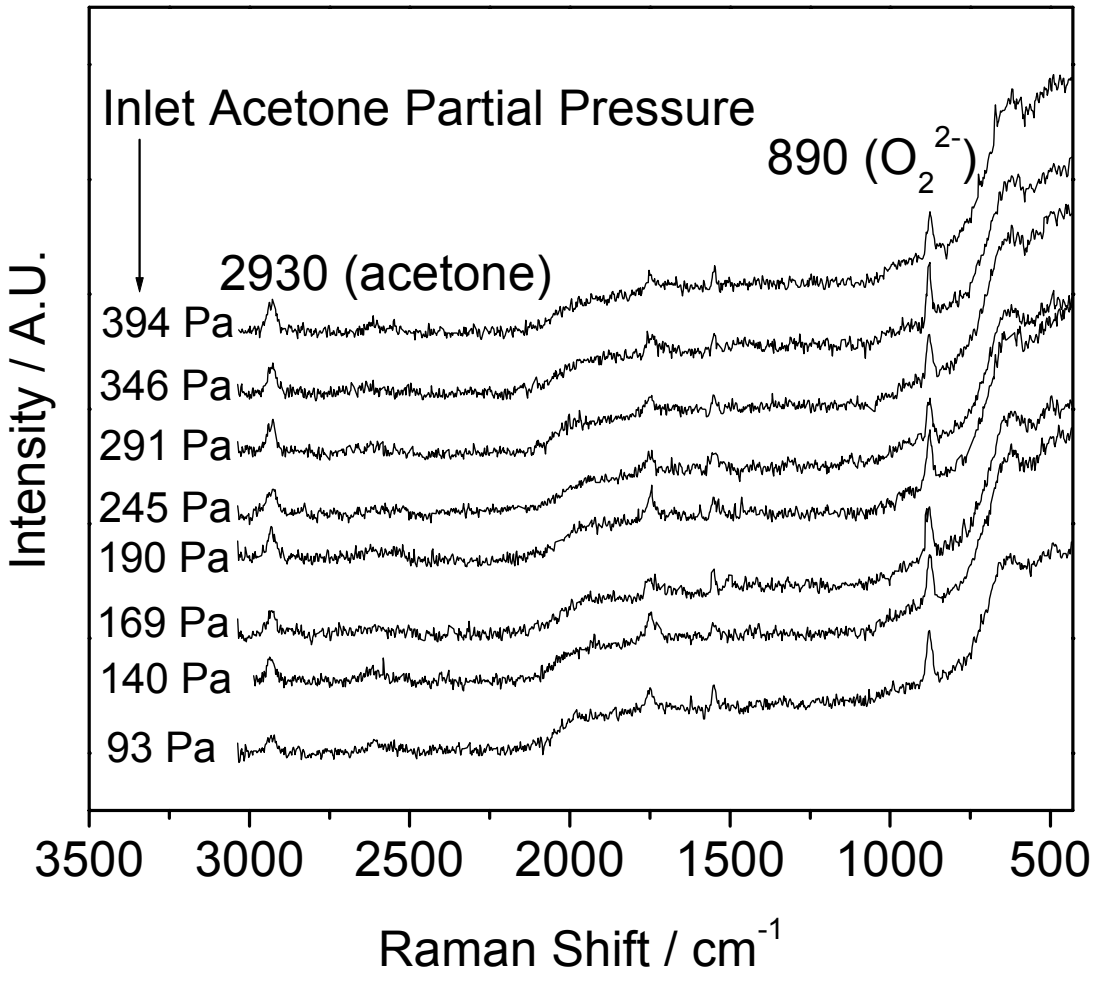

Figure 3.2. Steady-state Raman spectra taken at 318 K when acetone partial pressure is varied and ozone partial pressure is constant at ~790 Pa.

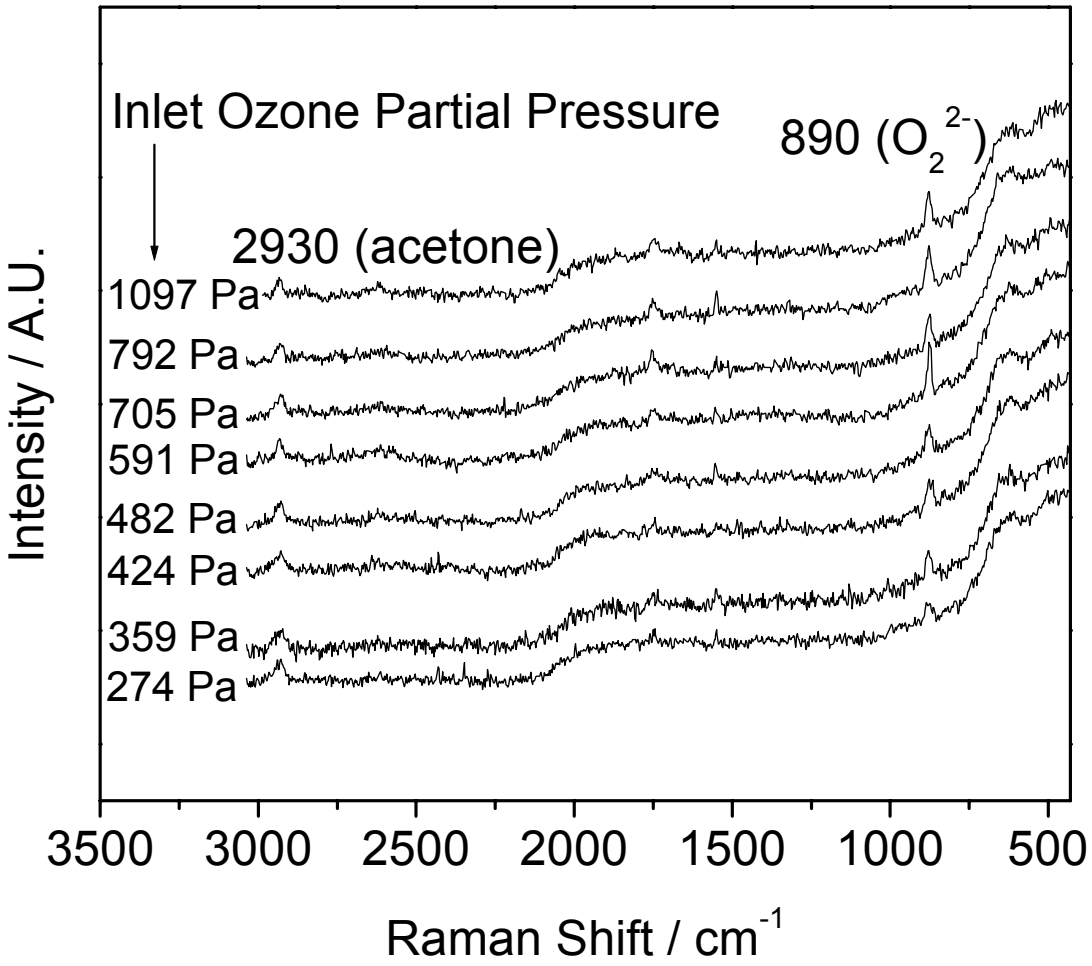

Figure 3.3. Steady-state Raman spectra taken at 318 K when ozone partial pressure is varied and acetone partial pressure is constant at ~193 Pa.

Figure 3.4 shows the coverage values associated with acetone (θ_A) and ozone (θ_{O2*}) when the initial acetone partial pressure was varied, and the initial ozone partial pressure was kept constant (790 Pa). Figure 3.5 shows the coverages associated with acetone (θ_A) and ozone (θ_{O2*}) when the initial ozone partial pressure was varied, and the initial acetone partial pressure was kept constant (193 Pa).

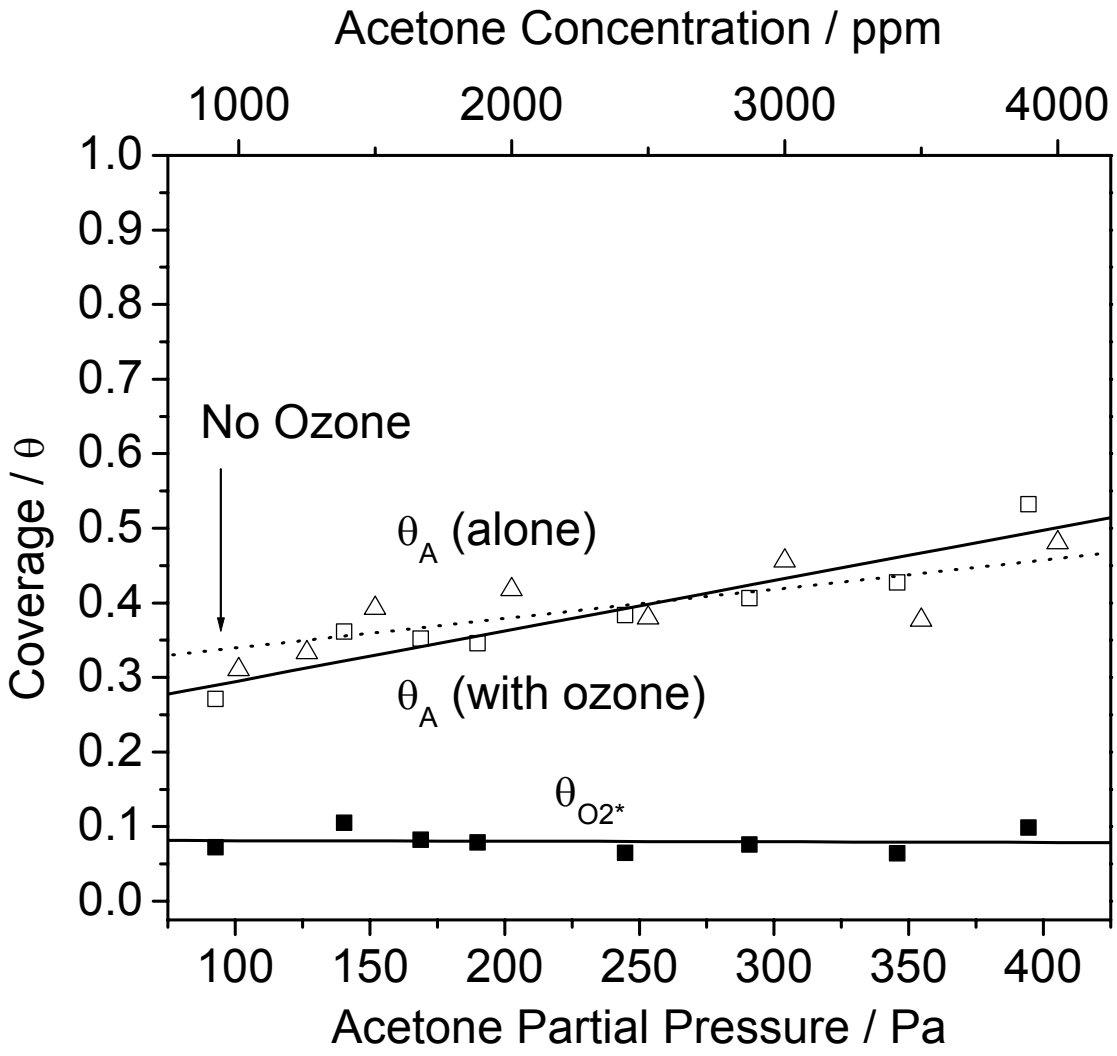

Figure 3.4. Steady-state surface coverage values at 318 K for adsorbed acetone and ozone intermediates when acetone partial pressure is varied and ozone partial pressure is constant at ~790 Pa.

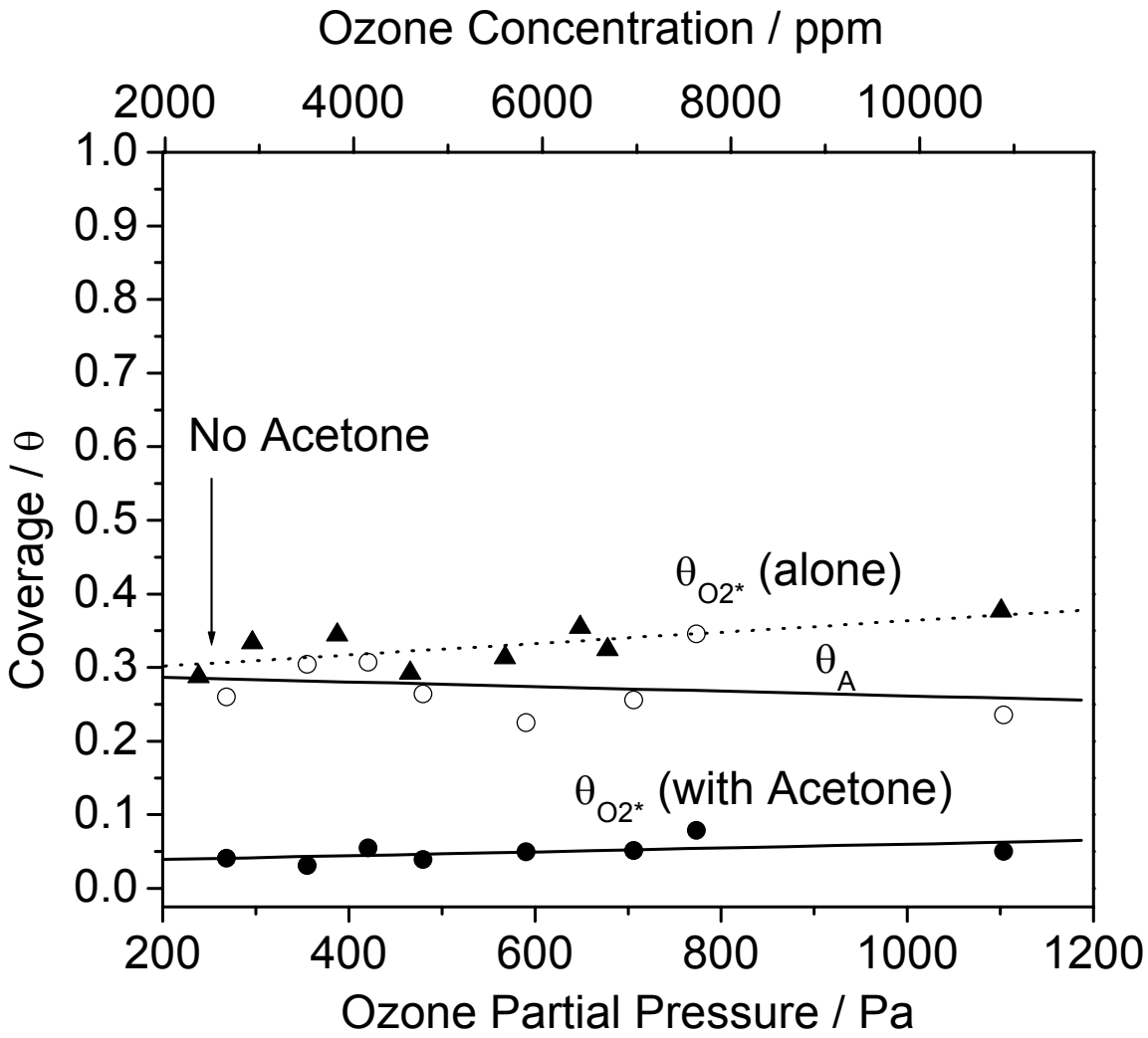

Figure 3.5. Steady-state surface coverage values at 318 K for adsorbed acetone and ozone intermediates when ozone partial pressure is varied and acetone partial pressure is constant at ~193 Pa.

3.3.3 Steady-State Kinetic Measurements

Kinetic experiments were performed to determine the rates of acetone and ozone reaction on the 10 wt. % MnO_x/SiO_2 catalyst sample. The data were obtained by varying one of the reactants (acetone or ozone) partial pressures over a range while maintaining the other reactant partial pressure close to the middle of the range. A blank kinetic

experiment was conducted to determine the gas-phase contributions to the oxidation reaction. The gas-phase conversions for both acetone and ozone were subtracted from those obtained from the experiments run with catalyst so that the calculated kinetic parameters accounted only for the reaction on the catalyst surface. The only observed product for the oxidation of acetone using ozone in the temperature range studied (333 – 373 K) was CO_2.

Using the conversions obtained for each reactant species, turnover frequencies (TOFs) for both acetone and ozone conversion were calculated based on the atomic oxygen uptake value (98 μmol/g) for the 10 wt. % MnO_x/SiO_2 catalyst sample. Figures 3.6 – 3.9 show the temperature and pressure dependencies of the acetone and ozone TOFs presented as logarithmic plots. For Figures 3.6a) – 3.9a), the straight lines displayed are overall fits for a power-law rate expression for both acetone and ozone TOF. For Figures 3.6b) – 3.9b), the curves displayed are fits for a derived Langmuir-Hinshelwood rate expression for both acetone and ozone TOF. The power rate law expressions were obtained by taking the concentration (mol/m^3), TOF (s^{-1}), and temperature (K) data and simultaneously fitting the entire data set by nonlinear least squares regression analysis using the program POLYMATH 5.1 [4] to obtain the kinetic parameters, which will be discussed in detail later. The Langmuir-Hinshelwood rate expressions were obtained by taking the concentration (mol/m^3), TOF (s^{-1}), and temperature (K) data for a single temperature and fitting each data set by nonlinear least squared regression analysis using the same program. The development of the Langmuir-Hinshelwood kinetic expression as well as a statistical comparison of the degree of fit for the two different rate expression forms will be discussed later.

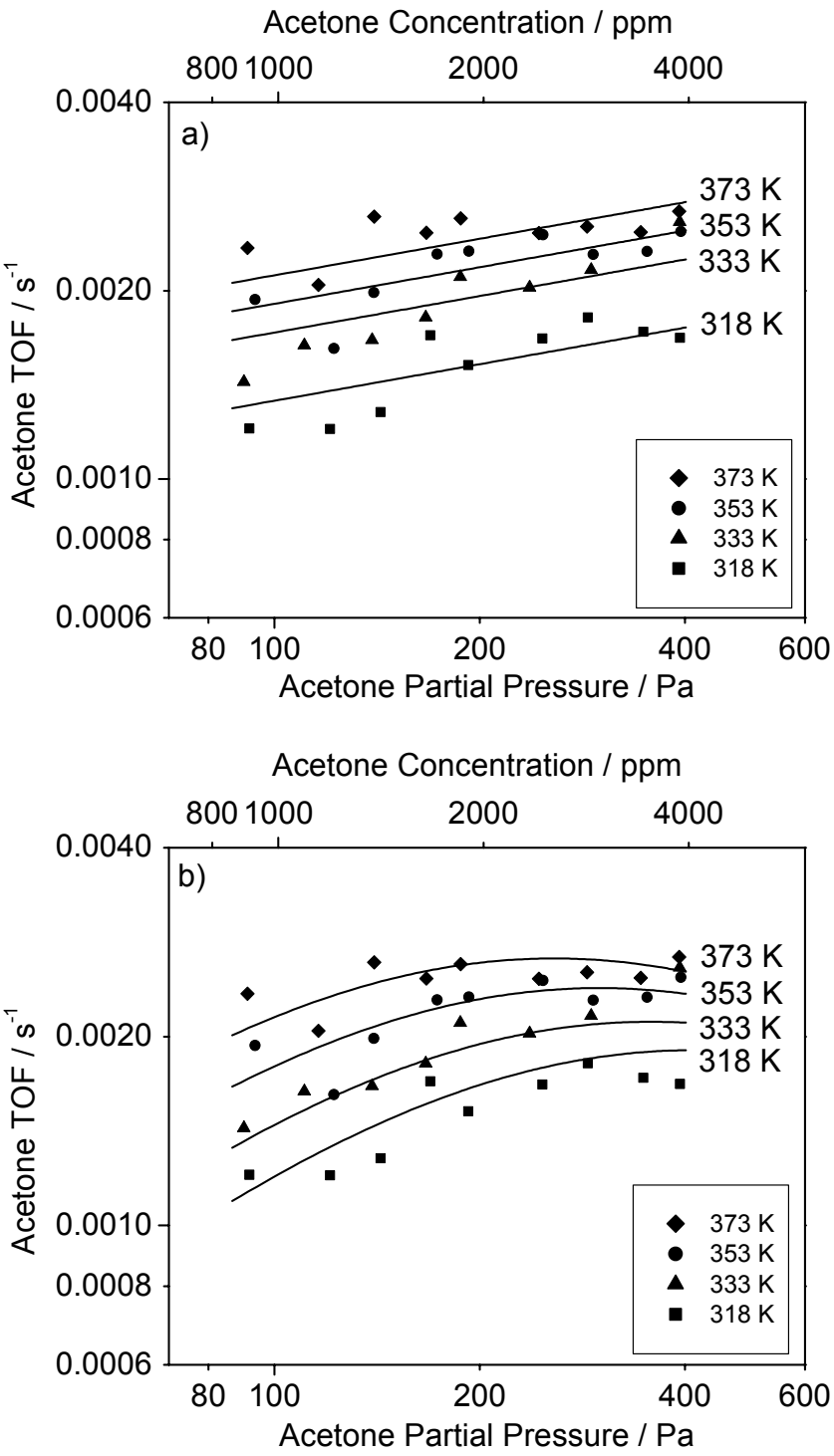

Figure 3.6. Steady-state kinetic data for acetone TOF as a function of acetone partial pressure when the partial pressure of ozone is constant at ~790 Pa for the a) power rate law expression and b) Langmuir-Hinshelwood expression.

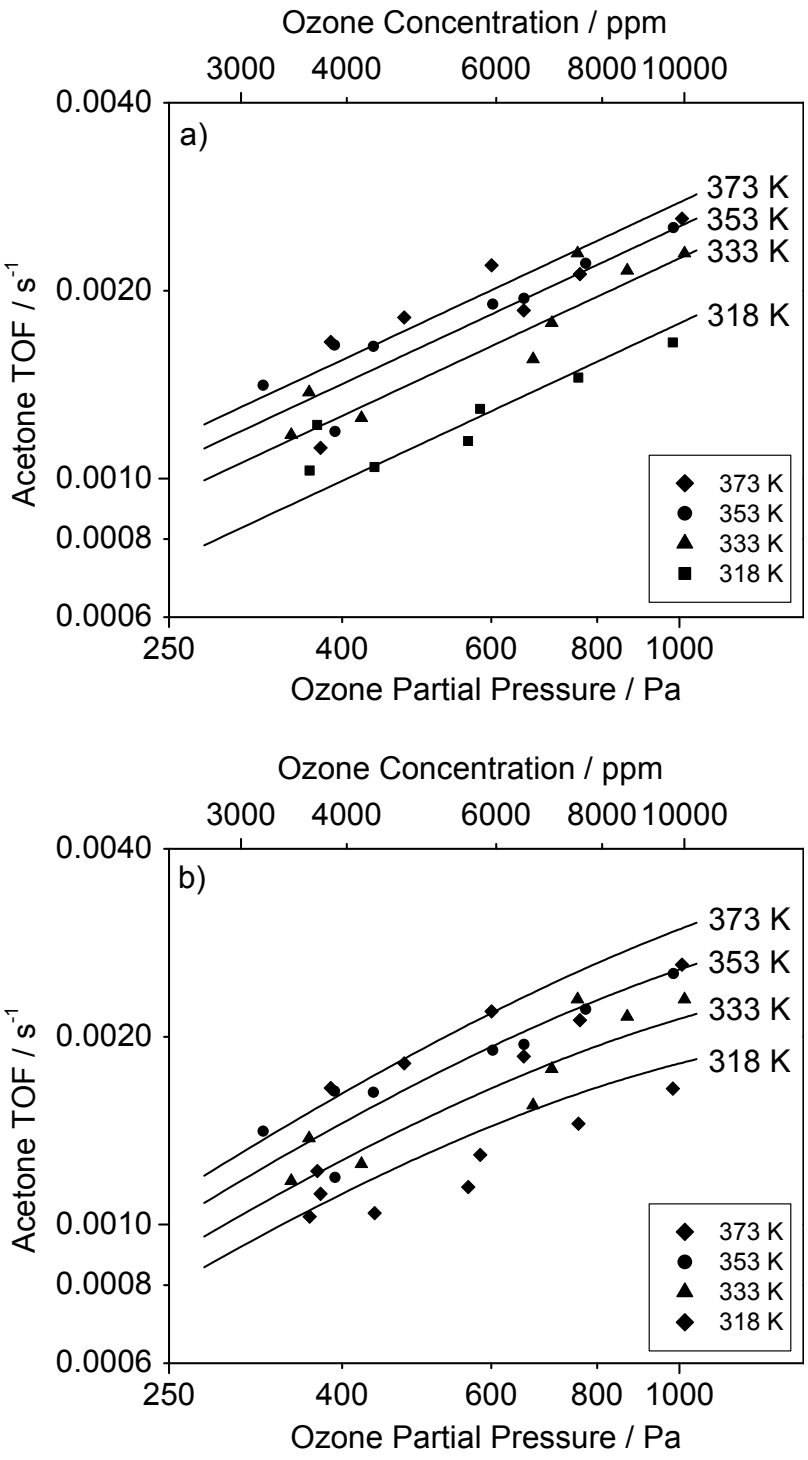

Figure 3.7. Steady-state kinetic data for acetone TOF as a function of ozone partial pressure when the partial pressure of acetone is constant at ~193 Pa for the a) power rate law expression and b) Langmuir-Hinshelwood expression.

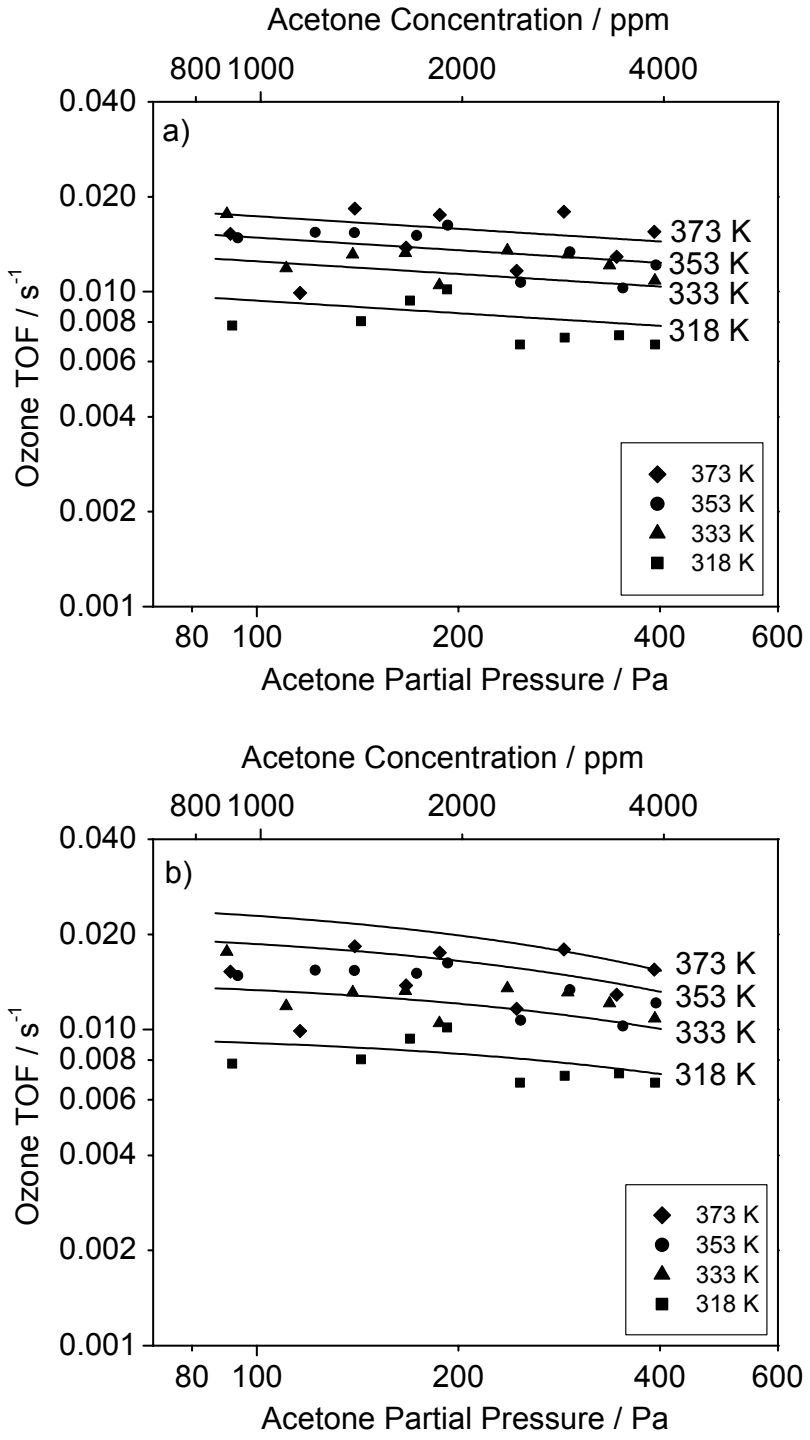

Figure 3.8. Steady-state kinetic data for ozone TOF as a function of acetone partial pressure when the partial pressure of ozone is constant at ~790 Pa for the a) power rate law expression and b) Langmuir-Hinshelwood expression.

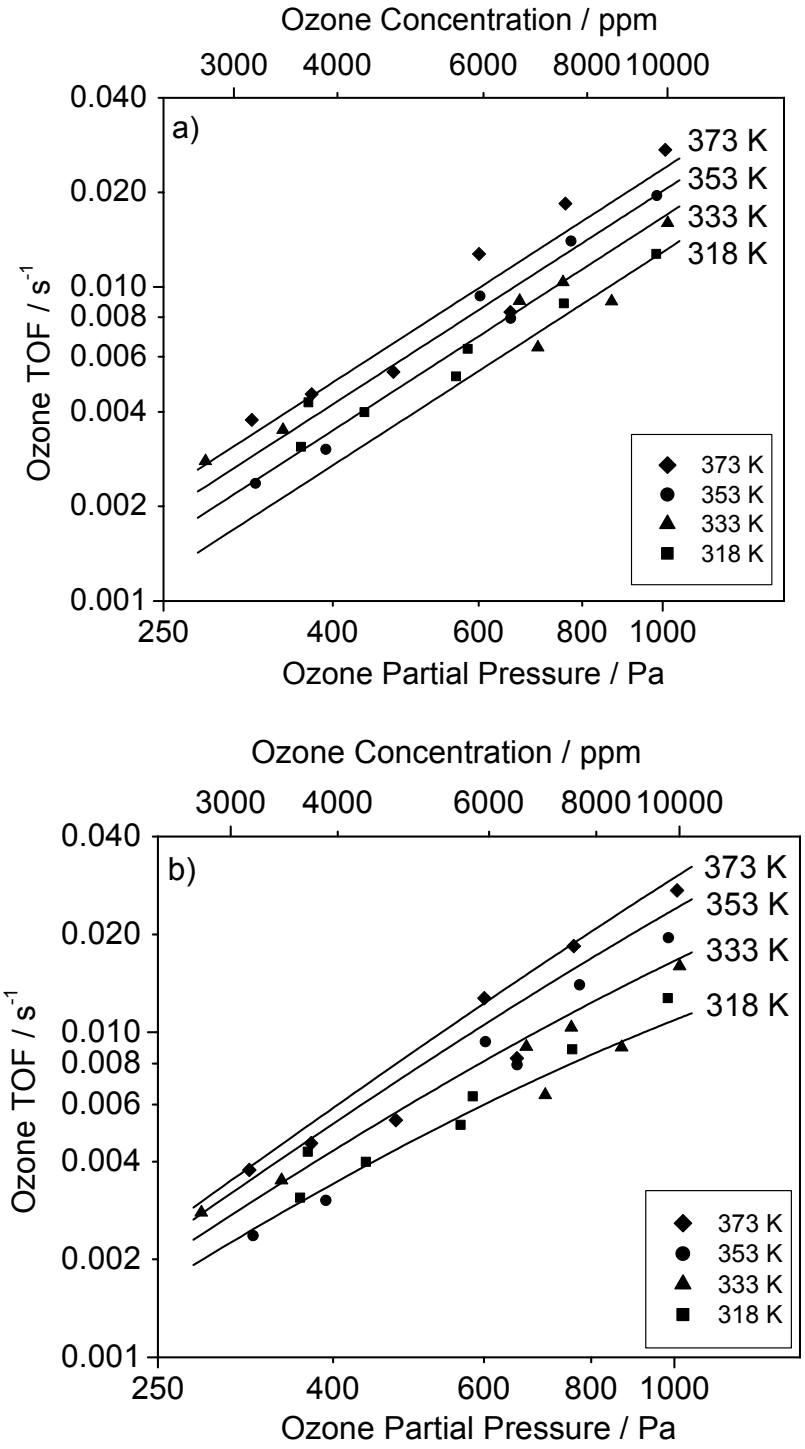

Figure 3.9. Steady-state kinetic data for ozone TOF as a function of ozone partial pressure when the partial pressure of acetone is constant at ~193 Pa for the a) power rate law expression and b) Langmuir-Hinshelwood expression.

3.3.4 Transient Kinetic Measurements

Transient, *in situ* Raman spectroscopy experiments were conducted on the 10 wt. % MnO_x/SiO_2 catalyst at 318 K using initial partial pressures for acetone and ozone of 193 and 793 Pa (1,900 and 7,800 ppm), respectively. Schematic depictions of these experiments are shown in Figure 3.10.

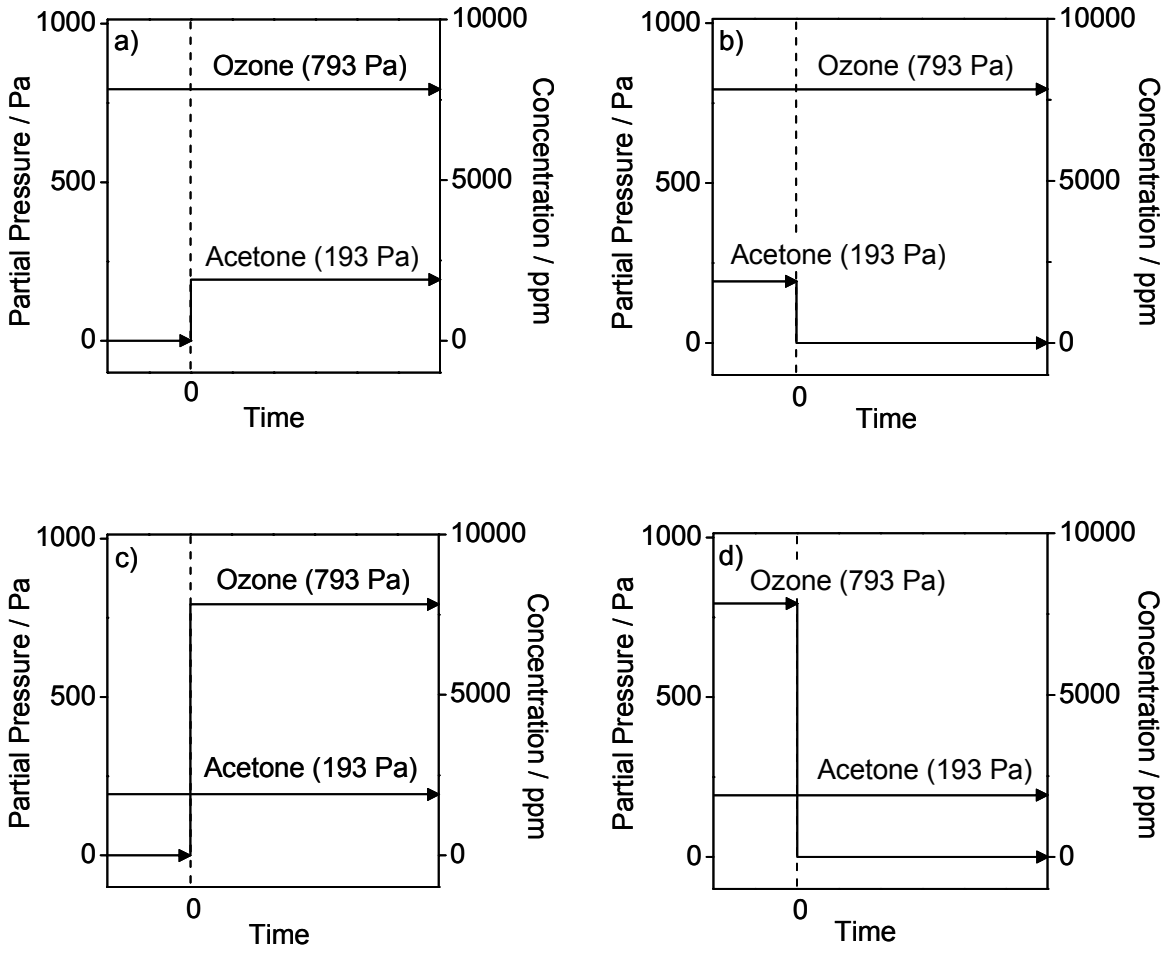

Figure 3.10. Schematic depictions of transient experiments, which include a) acetone addition, b) acetone removal, c) ozone addition, and d) ozone removal.

Transient experiments were utilized so that the rate of adsorption for each adsorbed intermediate could be studied separately from the rates of reaction and desorption. Figure 3.11 presents the acetone addition results and includes an inset describing the inlet partial pressure profiles for the experiment. As soon as acetone was introduced, the coverage associated with the peroxide species quickly dropped to a stable value of 0.08 in ~600 s while the coverage associated with the acetone intermediate increased to a steady value of 0.46 in ~900 s. Figure 3.12 shows the acetone removal results and also includes an inset describing for the experiment. When acetone was removed from the reaction mixture, the coverage associated with the peroxide species gradually increased and took over 3000 s to reach a value of 0.38 even though the coverage associated with the acetone intermediate decreased to zero in ~1250 s. Figure 3.13 presents the ozone addition results and the partial pressure profiles for the experiment. When ozone was introduced, the coverage associated with the peroxide species increased quickly to a steady value of 0.09 in ~800 s while the coverage associated with the acetone intermediate seemed to slightly decrease from an initial value of 0.49 to a final value of 0.42 over the time scale shown (~3000 s). Finally, Figure 3.14 shows the ozone removal results along with the partial pressure profiles for the experiment. When ozone was removed from the gas stream, the coverage associated with the peroxide species gradually decreased until no peroxide was detected at ~1950 s while the coverage associated with the acetone intermediate remained unchanged at 0.43.

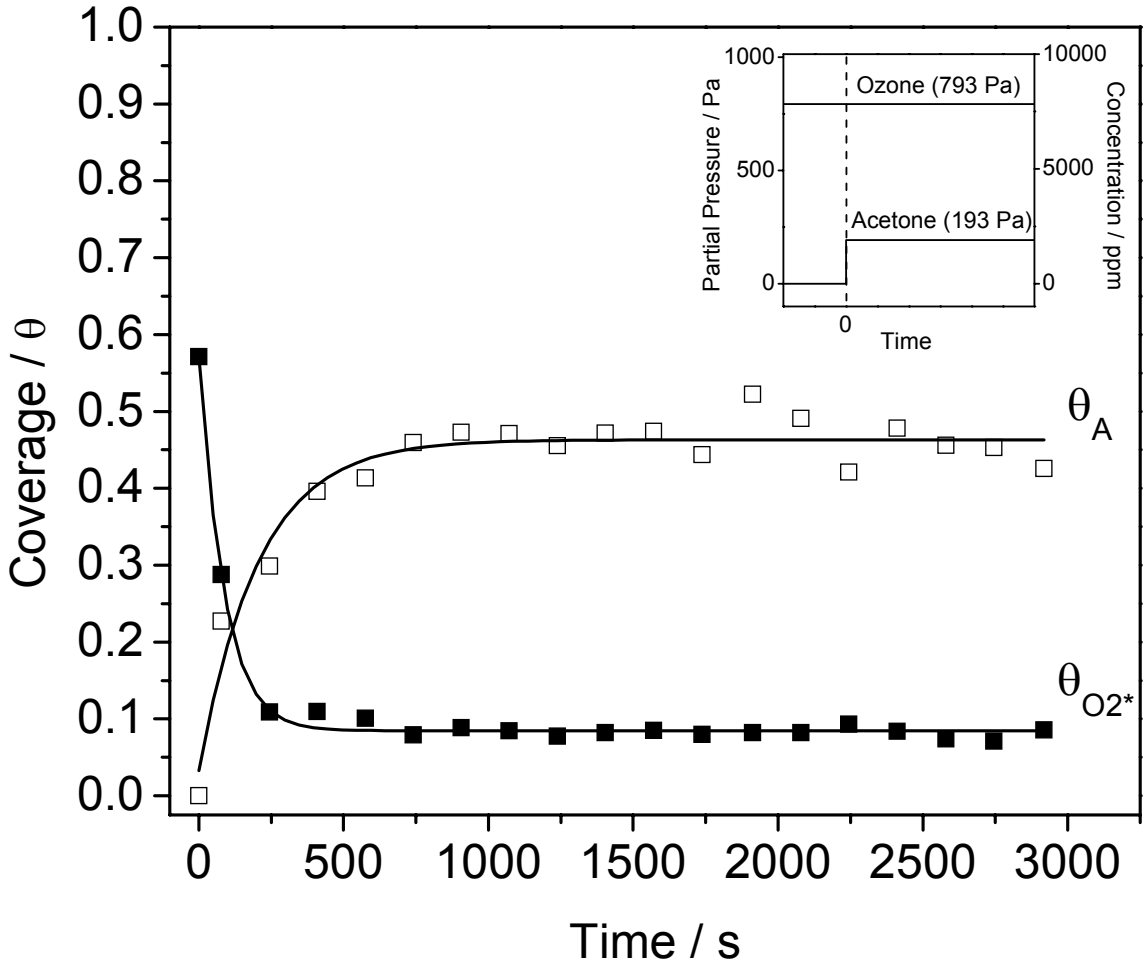

Figure 3.11. Transient acetone addition results at 318 K showing coverage values for adsorbed acetone and ozone intermediates as a function of time; Inset shows the inlet partial pressure profiles used for the experiment.

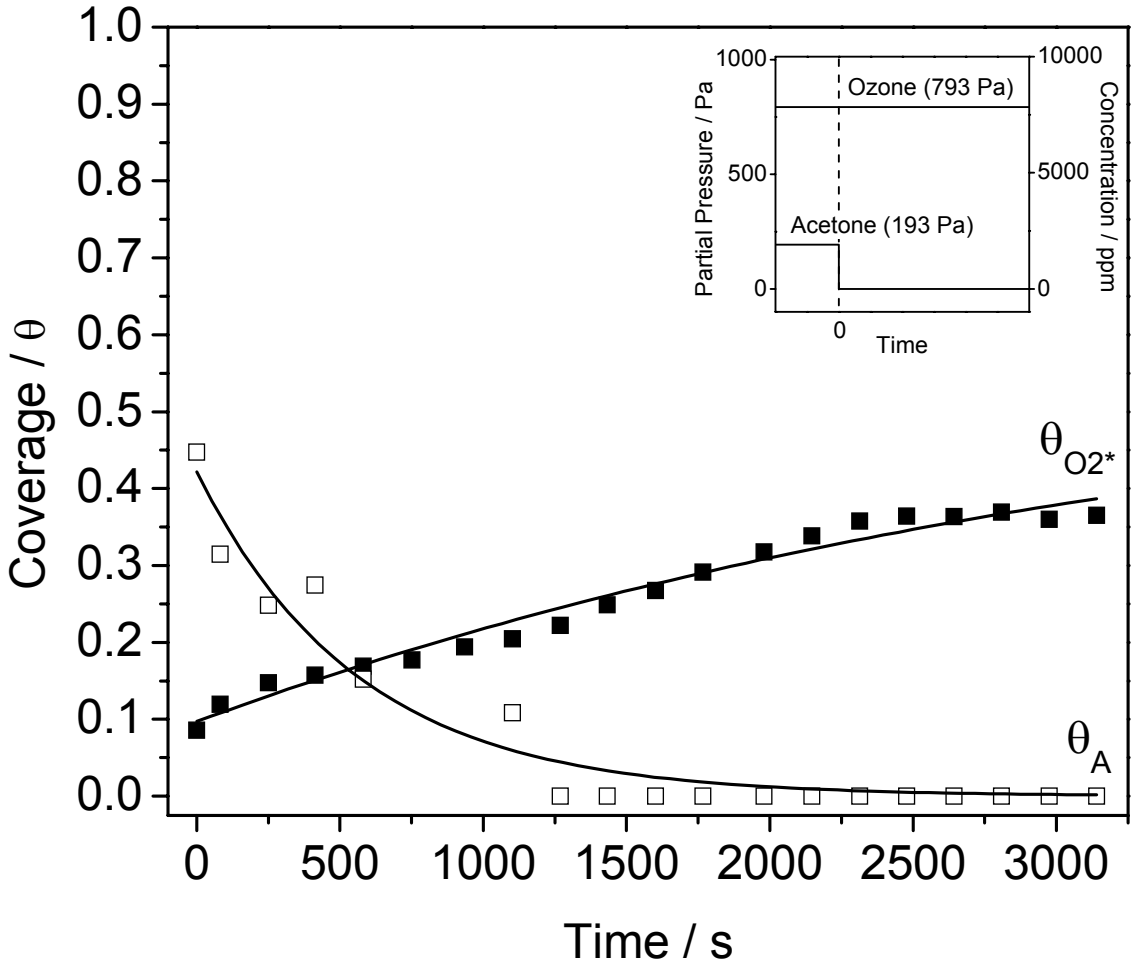

Figure 3.12. Transient acetone removal results at 318 K showing coverage values for adsorbed acetone and ozone intermediates as a function of time; Inset shows the inlet partial pressure profiles used for the experiment.

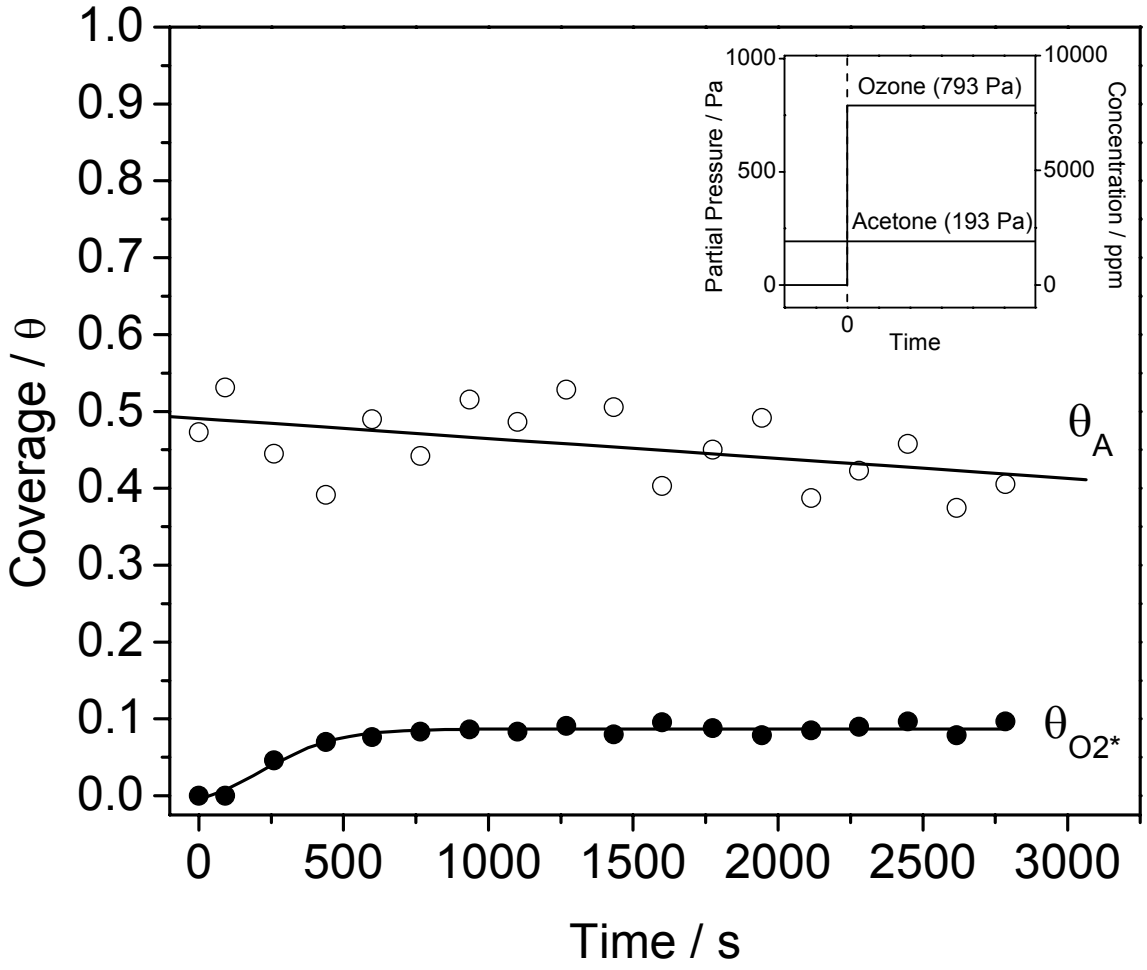

Figure 3.13. Transient ozone addition results at 318 K showing coverage values for adsorbed acetone and ozone intermediates as a function of time; Inset shows the inlet partial pressure profiles used for the experiment.

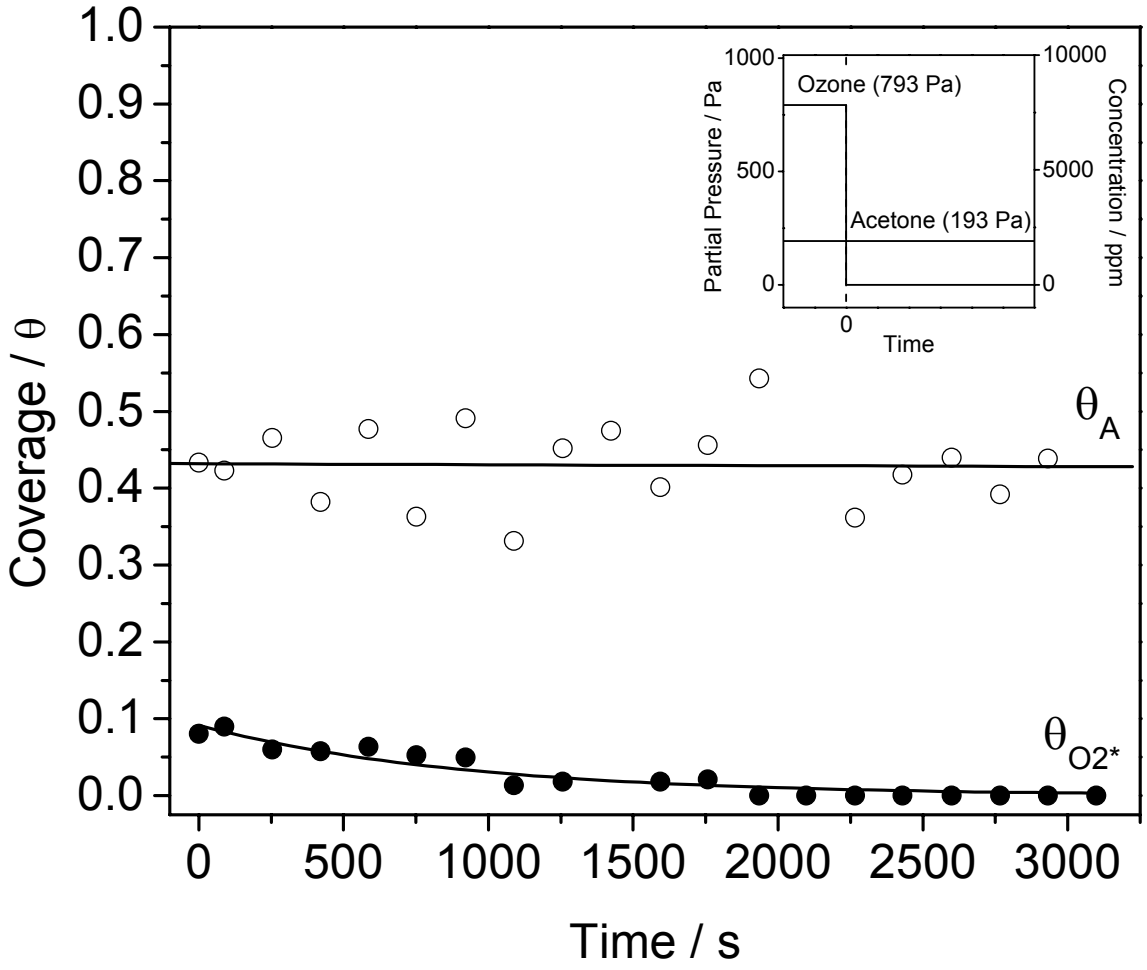

Figure 3.14. Transient ozone removal results at 318 K showing coverage values for adsorbed acetone and ozone intermediates as a function of time; Inset shows the inlet partial pressure profiles used for the experiment.

3.4 Discussion

3.4.1 Acetone Oxidation With Ozone

There are very few studies that have looked at the kinetics and mechanism of acetone oxidation. In one study [5] the mechanism of acetone oxidation over a preoxidized Ag (111) surface under ultrahigh vacuum (UHV) conditions was studied using reflection absorption IR. It was found that at 180 K, acetone adsorbs to form both propane-2,2-diyldioxy and acetone enolate via O-mediated nucleophilic addition and H abstraction. Once temperatures reached ~220 K, the acetone enolate was oxidized rapidly to produce transient metallacyclic intermediates and eventually stable ketenylidene and formate species. Isotopic labeling experiments showed that ketenylidene kept the acetone carbonyl group while the formate was formed from the acetone methyl group and surface O [5]. Another study [6] investigated the kinetics of the photocatalyzed oxidation of acetone (30 – 170 ppm) in air over a ceramic honeycomb monolith coated with TiO_2. It was found that the monolith adsorbed both acetone and water and that their coverages were described by a Langmuir adsorption isotherm for acetone and a modified BET adsorption isotherm for water. The rate expression for the disappearance of acetone took the form of a Langmuir-Hishelwood expression [6]. In a third study [7] the mechanism and kinetics of catalytic partial oxidation of acetone were investigated on vanadium pentoxide at 413 – 453 K. The main partial oxidation products were acetic acid, methanol, and carbon dioxide with minor amounts of formaldehyde and acetaldehyde. The order of the reaction for both acetone and oxygen ranged from zero to one while the activation energy was found to be ~75 kJ/mol, and the mechanism was

consistent with alternating redox steps. The data obtained agreed with the proposed mechanism and the derived kinetic expression except when the concentration of oxygen was varied, and it was concluded that the catalyst reoxidation step was complex [7].

3.4.2 Temperature Programmed Desorption (TPD) Measurements

The oxygen chemisorption measurements on the 10 wt. % MnO_x/SiO_2 catalyst reported in Chapter 2 gave the number of reduced surface manganese atoms on the supported catalysts to be 98 μmol/g. Dispersion values based on the atomic oxygen chemisorption measurements were compared to dispersion values based on x-ray diffraction (XRD) line-broadening results, and the two techniques gave very similar results. Thus, it was concluded that oxygen chemisorption measurements give a reasonable estimate of the number of surface manganese atoms. In this work, ozone TPD results gave a saturation peroxide adsorption value of 14 μmol/g. Thus, at maximum peroxide adsorption, only ~14 % of the surface manganese atoms adsorbed a peroxide species. Acetone TPD experiments, however, gave very different results. On the 10 wt. % MnO_x/SiO_2 catalyst, the saturation amount of acetone intermediate adsorbed on the catalyst surface was 550 μmol/g. Since this value was ~5.5 times the value obtained for the total number of surface manganese atoms, it can be concluded that most of the adsorbed acetone was located on the silica support. Acetone TPD experiments performed on pure silica resulted in a saturation adsorption value of 790 μmol/g. The BET surface area of the silica and the 10 wt. % MnO_x/SiO_2 sample were 320 and 210 m^2/g, respectively. Normalizing the acetone TPD results with respect to surface area gave maximum acetone adsorption values of 2.5 and 2.6 μmol/m^2 for both pure silica and the

10 wt. % MnO_x/SiO_2 sample, respectively (Table 3.1). Therefore, the amount of acetone adsorbed on the pure silica was essentially the same as the amount of acetone adsorbed on the 10 wt. % MnO_x/SiO_2 sample based on surface area. This further confirmed that most of the adsorbed acetone for the 10 wt. % MnO_x/SiO_2 catalyst was located on the silica support rather than the surface Mn atoms. Thus, although the coverages reported in this study are based on saturation adsorption, the coverages for the peroxide species are for occupation of the Mn sites, while the coverages for the acetone species are for occupation of the silica support.

3.4.3 Steady-State Raman Spectroscopy Measurements

Raman experiments done on pure, calcined silica and the 10 wt. % MnO_x/SiO_2 catalyst in acetone flow at 298 K are compared in Figure 3.1 to gain further understanding of the nature of acetone adsorption. Figure 3.1a) and 3.1b) show the Raman spectra for the 10 wt. % MnO_x/SiO_2 catalyst when acetone was included in the gas mixture at a concentration of 0.2 and 0.4 mol %, respectively. Figure 3.1c) and 3.1d) display the Raman spectra for the pure silica when the concentration of acetone was 0.2 and 0.4 mol %, respectively. The feature at 2930 cm^{-1} was attributed to the adsorbed acetone intermediate and was assigned to a CH_3 symmetric stretching mode from data in the literature [8].

Other bands associated with adsorbed acetone were also observed in the Raman spectra for pure silica. The features in Figure 3.1c) and 3.1d) located at 798 and 1710 cm^{-1} were assigned to a C-C stretching mode and a C-O stretching mode, respectively. These features observed for the adsorbed acetone intermediate on the pure silica sample

were close to those reported for gas-phase acetone using infrared spectroscopy with bands at 777, 1731, and 2937 cm^{-1} for C-C, C-O, and CH_3 stretching modes, respectively. The intensities for these features associated with gas-phase acetone were reported to be weak for the C-C stretching mode, very strong for the C-O stretching mode, and strong for the CH_3 stretching mode [8]. However, for the Raman experiments conducted, the feature (2930 cm^{-1}) attributed to a CH_3 stretching mode was significantly stronger in intensity than the feature (1710 cm^{-1}) attributed to a C-O stretching mode. This not only verifies that the acetone was adsorbed, but gives evidence that the molecularly adsorbed acetone intermediate bonds to the catalyst surface via the oxygen atom. Further Raman experiments conducted on the pure silica sample in acetone flow showed that heating to only 353 K resulted in a large decrease in peak intensities while further heating to just 393 K resulted in the complete disappearance of the bands. These experiments give additional confirmation that the acetone was physisorbed on the sample surface, for if the Raman features resulted from gas-phase acetone, they would not have decreased so drastically at these low temperatures. Also, these Raman results confirm that acetone adsorbed molecularly on the silica surface with retention of CH_3, C-O, and C-C stretching modes.

Another result from the Raman spectra displayed in Figure 3.1 is that the peak intensities and areas for the band located at 2930 cm^{-1} are much greater (~10×) for the pure silica sample compared to the 10 wt. % MnO_x/SiO_2 sample. Also, there are no observable bands located at 798 and 1710 cm^{-1} for the 10 wt. % MnO_x/SiO_2 sample. An initial conclusion resulting from these spectra would be that more acetone adsorbs on the pure silica than the 10 wt. % MnO_x/SiO_2 catalyst. However, it must be considered that

the surface area of the SiO_2 support (320 m^2g^{-1}) was larger than that of the catalyst (210 m^2g^{-1}) (Table 3.1) and that the white color of the pure silica sample results in clearer and more intense Raman signals compared to the dark (black) 10 wt. % MnO_x/SiO_2 sample. Therefore, the acetone TPD results should be reliable, and the conclusion that similar amounts of acetone, based on surface area, are adsorbed on both samples under the same conditions is firm. It was also observed that the acetone coverage was obtained in approaching a temperature from higher and lower values, indicating that the acetone adsorption was equilibrated.

Also, it is important to note that including ozone in the mixture gas for the Raman experiments on pure silica had no effect on the resulting spectra. Ozone was not seen to adsorb on the pure silica sample (Table 3.1), and ozone did not affect the peak intensity or area for the bands associated with the adsorbed acetone intermediate when both acetone and ozone were included in the reaction mixture.

Figures 3.2 and 3.3 display the spectra for the steady-state, *in situ* Raman spectroscopy experiments conducted on the 10 wt. % MnO_x/SiO_2 catalyst at 318 K using the same varying partial pressure conditions that were used in the steady-state kinetic experiments. Figure 3.2 shows the spectra when the acetone partial pressure was varied (93 – 394 Pa)) while Figure 3.3 shows the spectra when the ozone partial pressure was varied (274 – 1097 Pa). As the partial pressure of acetone was increased (Fig. 3.2), the peak intensity associated with the adsorbed acetone intermediate (2930 cm^{-1}) increased. However, the increase in acetone partial pressure had little effect on the peak intensity associated with the adsorbed peroxide species (890 cm^{-1}). As the partial pressure of ozone was increased (Fig. 3.3), the peak intensity associated with the adsorbed acetone

intermediate (2930 cm^{-1}) slightly decreased while the peak intensity associated with the adsorbed peroxide species slightly increased.

Surface coverages were calculated for the two adsorbed intermediates using the Raman spectra shown in Figures 3.2 and 3.3. Figure 3.4 displays the coverages associated with acetone (θ_A) and ozone (θ_{O2*}) when the acetone partial pressure was varied, and Figure 3.5 shows the coverages when the ozone partial pressure was varied. Figure 3.4 shows that the coverage of the acetone intermediate increased with increasing acetone partial pressure while the coverage of the peroxide species was essentially unchanged. Also shown in Figure 3.4 is the increase in coverage attributed to the acetone intermediate when the initial acetone partial pressure was increased, and ozone was absent from the reacting mixture. Interestingly, the coverage associated with the adsorbed acetone intermediate was very similar regardless of whether ozone was included in the reacting mixture. This is consistent with its adsorption being equilibrated. Figure 3.5 shows that the coverage of the acetone species decreased very slightly with increasing ozone partial pressure while the coverage of the peroxide intermediate increased also only slightly. Also presented in Figure 3.5 is the increase in coverage for the peroxide species when the initial ozone partial pressure was increased, and acetone was not included in the reacting mixture. Unlike the effect seen in the coverage of the acetone intermediate, the coverage for the adsorbed peroxide species was drastically reduced when acetone was included in the reaction mixture. All these observations are consistent with the adsorbed acetone and peroxide species being reaction intermediates. As will be seen, this is not the case.

3.4.4 Steady-State Kinetic Analysis

The reactivity study discussed in Chapter 2 that was performed on the 10 wt. % MnO_x/SiO_2 catalyst found that the oxidation reaction between acetone and ozone occurred in two different temperature regimes. At high temperatures (T > 475 K), the reaction was homogeneous and took place mainly in the gas-phase due to thermal decomposition of ozone, but at lower temperatures (T < 400 K), the reaction took place on the catalyst surface and resulted in a significant reduction in activation energies for both the acetone and ozone reactions. In this work, a detailed kinetic analysis was conducted in the lower temperature regime. The measurements were conducted in the apparatus shown in Figure 2.1, and only data at low conversions (< 10 %) were used in the analysis. The resulting kinetic data was used to determine the kinetic parameters (rate constants, equilibrium constants, activation energies, and orders of reaction for both reactants for two different types of rate expressions, a power rate law and a Langmuir-Hinshelwood expression.

The power rate law model had four unknown parameters (A, E_a, α, β) and took the form,

$$TOF = A\exp\left(\frac{-E_a}{RT}\right)C_A^{\alpha}C_{O3}^{\beta}, \tag{3.1}$$

where TOF is the turnover frequency, A is the frequency factor, E_a is the apparent activation energy, R is the gas constant, T is the temperature (K), C_A is the concentration of acetone (mol/m^3), C_{O3} is the concentration of ozone (mol/m^3), and α and β are the orders with respect to acetone and ozone concentration, respectively.

To determine the rate expression for acetone conversion, the entire data set, consisting of the concentrations of both reactants, acetone TOFs, and all temperatures,

was simultaneously fit to an expression of the form shown above using nonlinear least squares regression analysis (Figs. 3.6a) – 3.9a)). The rate of acetone conversion using all the data was found to be:

$$Acetone\ TOF = 0.0797 \exp\left(\frac{-7.05\ kJ/mol}{RT}\right) C_A^{0.194} C_{O3}^{0.634} \tag{3.2}$$

The fitting analysis resulted in a R^2 degree of fit and variance values of 0.834 and 5.16×10^{-7}, respectively. The data for each temperature was then regressed using a common slope based on the overall fit shown above. When acetone TOF was varied with respect to acetone partial pressure, the slope ($\alpha = 0.194$) was held constant, and when acetone TOF was varied with respect to ozone partial pressure, the slope ($\beta = 0.634$) was held constant. The lines in Figures 3.6a) and 3.7a) show the individual, regressed fits at each temperature for the power rate law expressions for acetone TOF against the actual kinetic data.

The rate expression for ozone conversion was found in the same manner as the rate expression for acetone conversion. The rate of ozone conversion using all the data was found to be:

$$Ozone\ TOF = 2.04 \exp\left(\frac{-10.0\ kJ/mol}{RT}\right) C_A^{-0.133} C_{O3}^{1.71} \tag{3.3}$$

The fitting analysis resulted in a R^2 degree of fit and variance values of 0.823 and 5.73×10^{-5}, respectively. As was done for the fits for acetone TOF, the data for each temperature was regressed using a common slope based on the overall fit for ozone TOF. Figures 3.8a) and 3.9a) display the individual, regressed fits at each temperature for the power rate law expressions for ozone TOF against the actual kinetic data. The entire

fitting results and statistical parameters for the power rate law rate expressions are shown in Table 3.2.

The power rate law expressions proposed show that the calculated activation energies for acetone and ozone conversion are 7.1 and 10.0 kJ/mol, respectively. These values compare favorably with activation energies found from the reactivity study presented in Chapter 2 done on the same 10 wt. % MnO_2/SiO_2 catalyst sample for the reaction between acetone and ozone. For temperatures less than 400 K, the study reported an activation energy for acetone conversion of 7.3 kJ/mol and an activation energy for ozone conversion of 13.8 kJ/mol. Thus, the similarity in activation energies for these two studies confirms that in this temperature range, the reaction takes place mainly on the catalyst surface.

Table 3.2. Non-linear least squared regression results for the kinetic data utilizing the power rate law expressions.

Power rate law expression: $Acetone\ TOF = A\exp\left(\frac{-E_a}{RT}\right)C_A^{\alpha}C_{O3}^{\beta}$						
T / K	A	E_a / kJ mol^{-1}	α	β	R^2	variance
318, 333, 353, 373	0.0797	7.05	0.194	0.634	0.834	5.16×10^{-7}
318 – vary acetone	0.0700	7.37	0.194	0.482	0.789	2.10×10^{-7}
333 – vary acetone	0.0799	7.03	0.194	0.595	0.805	4.75×10^{-7}
353 – vary acetone	0.0759	7.18	0.194	0.539	0.827	3.88×10^{-7}
373 – vary acetone	0.0846	6.86	0.194	0.750	0.799	8.04×10^{-7}
318 – vary ozone	0.0843	6.89	0.266	0.634	0.774	2.25×10^{-7}
333 – vary ozone	0.0968	6.48	0.331	0.634	0.856	3.32×10^{-7}
353 – vary ozone	0.0807	7.01	0.195	0.634	0.810	4.24×10^{-7}
373 – vary ozone	0.0690	7.61	0.091	0.634	0.771	7.60×10^{-7}
Power rate law expression: $Ozone\ TOF = A\exp\left(\frac{-E_a}{RT}\right)C_A^{\alpha}C_{O3}^{\beta}$						
T / K	A	E_a / kJ mol^{-1}	α	β	R^2	variance
318, 333, 353, 373	2.04	10.0	-0.133	1.71	0.823	5.73×10^{-5}
318 – vary acetone	1.52	10.8	-0.133	1.27	0.812	1.70×10^{-5}
333 – vary acetone	1.71	10.5	-0.133	1.37	0.745	5.85×10^{-5}
353 – vary acetone	2.02	10.1	-0.133	1.68	0.859	4.31×10^{-5}
373 – vary acetone	2.36	9.57	-0.133	1.98	0.769	1.23×10^{-4}
318 – vary ozone	1.98	10.1	-0.133	1.71	0.761	2.16×10^{-5}
333 – vary ozone	1.87	10.3	-0.209	1.71	0.733	6.11×10^{-5}
353 – vary ozone	1.73	10.5	-0.264	1.71	0.888	3.69×10^{-5}
373 – vary ozone	2.34	9.53	-0.005	1.71	0.776	1.19×10^{-4}

Langmuir-Hinshelwood kinetic rate expressions were also derived from a proposed mechanism detailing the acetone oxidation reaction with ozone over the catalyst. Even though there may be other steps involved in the actual mechanism, many of the proposed steps have been verified and will be discussed. The proposed mechanism is as follows:

$$O_3 + * \longrightarrow O_2 + O* \quad (3.4)$$

$$O_3 + O* \longrightarrow O_2 + O_2* \quad (3.5)$$

$$O_2* \longrightarrow O_2 + * \quad (3.6)$$

$$A + \square \rightleftharpoons A\square \quad (3.7)$$

$$A\square + * \rightleftharpoons A* + \square \quad (3.8)$$

$$A* + nO* \longrightarrow \text{products} \quad (3.9)$$

where * represents a surface manganese site, □ represents a surface silica site, and A represents acetone (CH_3COCH_3).

The first three steps of the proposed mechanism are well understood for ozone decomposition on manganese oxide based on kinetic, spectroscopic, ab initio calculations, and isotopic substitution [2,3]. Even though these steps have been verified, they will be briefly explained here. Raman spectroscopy was used to identify a band at 884 cm^{-1} that appeared during the decomposition reaction of ozone, and isotopic substitution experiments allowed the identification of the 884 cm^{-1} peak as belonging to a surface peroxide species (O_2^{2-}). This assignment was confirmed through ab initio calculations done on a model $Mn(OH)_4(O_2)$ complex that resulted in a vibrational frequency of 899 cm^{-1} that was in excellent agreement with the frequency observed in the spectroscopic experiments. Isotopic substitution experiments demonstrated that the peroxide species

was formed through atomic oxygen species, thus rationalizing the first two steps (Eqs. 3.4 and 3.5) of the proposed mechanism. The third step (Eq. 3.6) was verified by removing ozone from the reaction gas mixture, and observing the gradual decay in the peroxide signal (884 cm^{-1}) with time. This final step for ozone decomposition, where the peroxide species decomposes to form gas-phase molecular oxygen, is a slow step and was shown to be irreversible as reactions with oxygen alone did not form the adsorbed peroxide species at any condition [2].

It is known from the Raman experiments that even during the reaction with acetone, an adsorbed peroxide species is observed on the catalyst surface at 890 cm^{-1}. It is reasonable that this adsorbed peroxide species is formed in the same way as in the ozone decomposition reaction. Also, in the temperature range used for the kinetic analysis, the TOFs for the ozone were about 10× larger than the TOFs for the acetone reaction. Therefore, a reasonable, overall stoichiometry for the reaction between acetone and ozone is as follows,

$$CH_3COCH_3 + 8O_3 \longrightarrow 3CO_2 + 3H_2O + 8O_2, \qquad (3.10)$$

where each ozone molecule contributes a single oxygen equivalent to the reaction and produces an oxygen molecule. From the rate of ozone usage, it can be concluded that the decomposition of ozone takes place simultaneously with the oxidation reaction. Validation of the fourth step (Eq. 3.7) comes through the acetone TPD results, which demonstrated that nearly all the adsorbed acetone was located on the silica support. Raman spectroscopy experiments conducted on a pure silica sample in acetone flow (Fig. 3.1) confirmed that the silica had a strong affinity for acetone at low temperatures (< 373 K). The Raman studies identified an adsorbed acetone intermediate with a CH_3

symmetric stretching mode at 2930 cm^{-1}, a C-C stretching mode at 798 cm^{-1}, and a C-O stretching mode at 1710 cm^{-1} which gave evidence that the acetone was adsorbed molecularly since the C-H bonds were intact.

Most likely the silica support acted as a reservoir for the adsorbed acetone intermediates until reaction, when the adsorbed acetone migrated to an active Mn center (Eq. 3.8) and then reacted with an atomically adsorbed oxygen species to form products as is shown in the last step (Eq. 3.9) of the proposed mechanism. There is evidence that the adsorbed acetone intermediate reacts with an adsorbed atomic oxygen species rather than the adsorbed peroxide species. As will be discussed later in detail, transient kinetic experiments prove that the adsorbed peroxide species is a spectator in the acetone oxidation reaction, and therefore, an adsorbed atomic oxygen species is the likely reactive intermediate. These atomic oxygen species are highly reactive, quickly converting to peroxide species in the absence of acetone and are not observed. Raman experiments on the 10 wt. % MnO_x/SiO_2 catalyst show a dramatic decrease in the concentration of the peroxide intermediate with the characteristic band at 890 cm^{-1} when acetone is added to the reaction mixture. Initially, it might appear that acetone competes for active catalyst sites causing the amount of adsorbed peroxide species associated with ozone to decrease. However, a more reasonable explanation is that the atomic oxygen species, produced in the first step of the proposed mechanism (Eq. 3.4), are immediately used in the acetone oxidation reaction (Eq. 3.9), and therefore, less of these species are available for peroxide formation (Eq. 3.5). This then leads to the observed decrease in peroxide coverage when acetone is included in the reaction mixture as is shown in Figure 3.5.

Raman spectroscopy experiments also aided in determining that Eqs. 3.7 and 3.8 were equilibrated based on the observation of rapid decay and recovery of the adsorbed acetone coverage when acetone was removed from or added to the gas mixture. Also, the acetone coverage for a given set of conditions was always constant despite approaching from a lower or higher temperature further confirming the equilibrium of acetone adsorption. Acetone TPD experiments done on the 10 wt. % MnO_x/SiO_2 catalyst confirmed the reversibility of Eq. 3.7 since gas-phase acetone was the only desorption product observed.

The last step consists of a dual site reaction between an adsorbed acetone intermediate and an adsorbed atomic oxygen species resulting eventually in complete oxidation. This step can be considered as a slow step for the acetone reaction. It is followed by a series of fast steps (not shown) involving reactive acetone fragments and active oxygen species from ozone that produce the CO_2 observed as the reaction product.

Based on the proposed mechanism, rate expressions of the Langmuir-Hinshelwood type were developed for the rate of disappearance of both acetone and ozone. The adsorbed species on the manganese oxide were assumed to be the peroxide species observed in the Raman experiments and an acetone species. Eq. 3.9 was used to develop the rate of acetone disappearance giving the expression,

$$-r_A^{'} = r_6 = k_6 (A^*)(O^*)^n \tag{3.11}$$

The concentration of the adsorbed peroxide species was obtained by assuming $r_1 = r_3$,

$$(O_2{}^*) = \frac{k_1}{k_3}(O_3)(^*), \qquad \backslash \tag{3.12}$$

where k_1 is the rate constant for the first step (Eq. 3.4), k_3 is the rate constant for the third step (Eq. 3.6), and (*) is the concentration of vacant catalyst sites. The concentration of the adsorbed acetone species was obtained assuming the forth and fifth steps (Eqs. 3.7 and 3.8) are in equilibrium,

$$(A^*) = K_4 K_5 (A)(*), \tag{3.13}$$

where K_4 and K_5 are the equilibrium adsorption constants for the forth and fifth steps, respectively. Performing a total manganese site balance and assuming that the concentration of adsorbed atomic oxygen, (O*), is very small compared to the other adsorbed intermediates, the concentration of vacant sites, (*), can be determined to be,

$$(*) = \frac{(L)}{1 + \frac{k_1}{k_3}(O_3) + K_4 K_5 (A)} = \frac{(L)}{1 + k''(O_3) + K(A)}, \tag{3.14}$$

where (L) is the total concentration of active catalyst sites. The assumption that the concentration of adsorbed atomic oxygen is much less than that of the other adsorbates is justified considering that Raman spectroscopy did not identify a feature attributed to that intermediate. Therefore, the Langmuir-Hinshelwood rate expressions takes the form:

$$-r_A' = \frac{k'(A)(O_3)^n}{[1 + k''(O_3) + K(A)]^{1+n}} \tag{3.15}$$

$$-r_{O3}' = \frac{k'''(O_3)^2}{[1 + k''(O_3) + K(A)]^2} \tag{3.16}$$

In order to simplify the rate of acetone disappearance, the variable n was set equal to one assuming that one adsorbed acetone intermediate reacts with one adsorbed peroxide species in the last step (Eq. 3.9) of the proposed mechanism. This assumption is reasonable and results in a squared term in the denominator of the expressions, which is

typical for such a dual site mechanism. Both of the derived Langmuir-Hinshelwood rate expressions for the disappearance of acetone and ozone have three unknown parameters. Unlike the power rate law rate expressions, these Langmuir-Hinshelwood kinetic expressions do not include a temperature term. Therefore, to determine the rate for acetone disappearance, the data set specific to one temperature, consisting of the concentrations of both reactants and acetone TOFs, was simultaneously fit to the expression for $-r_A$' shown above using nonlinear least squares regression analysis. The fitting procedure was then repeated for each reaction temperature (318, 333, 353, and 373 K). Once the kinetic parameters (*k'*, *k"*, and *K*) were calculated for each temperature, they were regressed using the Arrhenius (*k'* and *k"*) or van't Hoff (*K*) equations to determine expressions for each kinetic parameter as a function of temperature. These expressions were then substituted into the Langmuir-Hinshelwood rate expression for acetone to determine an overall fit as a function of temperature.

$$-r_A^{'} = \frac{28.0\exp\left(\frac{-1350}{T}\right)(A)(O_3)}{\left[1+0.413\exp\left(\frac{532}{T}\right)(O_3)+133\exp\left(\frac{-818}{T}\right)(A)\right]^2} \tag{3.17}$$

Similarly, to determine the rate of ozone disappearance, the data set specific to one temperature, consisting of concentrations of both reactants and ozone TOFs, was simultaneously fit the expression for $-r_{O3}$' shown above using nonlinear regression analysis. This fitting procedure was again repeated for each reaction temperature (except 373 K), and the resulting kinetic parameters (k" and K) were regressed using the Arrhenius and van't Hoff equations. The k'" was regressed using only the fits at 318 and

333 K. The resulting Langmuir-Hinshelwood expression for the rate of ozone as a function of temperature is shown below.

$$-r'_{O3} = \frac{0.730 \exp\left(\frac{-262}{T}\right)(O_3)^2}{\left[1 + 7.66 \times 10^{-5} \exp\left(\frac{3320}{T}\right)(O_3) + 7.84 \exp\left(\frac{-456}{T}\right)(A)\right]^2} \quad (3.18)$$

Table 3.3 present the fitting results for the derived Langmuir-Hinshelwood rate expression based on the proposed mechanism, including statistical parameters while Figures. 3.6b) – 3.9b) show the fits with respect to the actual kinetic data.

Comparing Tables 3.2 and 3.3, the fitting statistic values (R^2 and variance) for the power rate law rate expressions and the Langmuir-Hinshelwood rate expressions are quite similar and cannot be used to discriminate between the rate expressions. Even though the variances calculated for the ozone rates are an order of magnitude smaller for the Langmuir-Hinshelwood expression compared to the power rate law, the R^2 degree of fits are comparable. The Langmuir-Hinshelwood expression for the rate of acetone disappearance gives reasonable kinetic parameters and fits, and thus, the proposed mechanism does match the data for the acetone reaction. The Langmuir-Hinshelwood expression for the disappearance of ozone also gives reasonable fits even though one of the optimized parameters (k" at 373 K, Table 3.3) is physically not realistic.

Overall, both the power rate law and Langmuir-Hinshelwood expressions give reasonable fits for the rates of disappearance of acetone and ozone. Based on the statistics for the fits as well as the kinetic parameters obtained, it is difficult to determine which of the two models better describes the data. The reasonable kinetic fits resulting from the Langmuir-Hinshelwood expressions provide further verification of the proposed

mechanism. Since all the steps included in the mechanism have been verified through experiment and have been confirmed through the fitting of actual kinetic data, it can be concluded that the mechanism provides insight into the molecular level processes occurring in the reaction of acetone and ozone over manganese oxide.

Table 3.3. Non-linear least squared regression results for the kinetic data utilizing the Langmuir-Hinshelwood expressions.

Langmuir-Hinshelwood expression: $Acetone\ TOF = \dfrac{k'(A)(O_3)}{\left[1 + k''(O_3) + K(A)\right]^2}$

T / K	k' / s^{-1} $(m^3/mol)^2$	k'' / $m^3\ mol^{-1}$	K / $m^3\ mol^{-1}$	R^2	variance
318	0.454	2.44	11.7	0.829	1.70×10^{-7}
333	0.396	1.59	9.07	0.851	3.64×10^{-7}
353	0.706	2.31	13.6	0.842	3.55×10^{-7}
373	0.744	1.61	15.5	0.720	7.51×10^{-7}
Regression	$28.0\exp\left(\dfrac{-11.2\,kJ\,mol^{-1}}{RT}\right)$	$0.413\exp\left(\dfrac{4.43\,kJ\,mol^{-1}}{RT}\right)$	$133\exp\left(\dfrac{-6.80\,kJ\,mol^{-1}}{RT}\right)$		

Langmuir-Hinshelwood expression: $Ozone\ TOF = \dfrac{k'''(O_3)^2}{\left[1 + k''(O_3) + K(A)\right]^2}$

T / K	k''' / s^{-1} $(m^3/mol)^2$	k'' / $m^3\ mol^{-1}$	K / $m^3\ mol^{-1}$	R^2	variance
318	0.320	2.40	2.13	0.820	1.32×10^{-6}
333	0.332	1.84	1.58	0.728	5.09×10^{-6}
353	0.289	0.864	2.40	0.892	2.88×10^{-6}
373	0.156	-0.0446	0.218	0.786	9.32×10^{-6}
Regression	$0.730\exp\left(\dfrac{-2.18kJ\,mol^{-1}}{RT}\right)$	$7.66\times10^{-5}\exp\left(\dfrac{27.6kJ\,mol^{-1}}{RT}\right)$	$7.84\exp\left(\dfrac{-3.79\,kJ\,mol^{-1}}{RT}\right)$		

3.4.5 Transient Kinetic Analysis

Even though it is important to identify the reactive intermediates involved in a catalytic reaction in order to elucidate a mechanism, it is equally important to recognize that not always do observed adsorbed species play a role in the overall catalytic cycle [9]. Sometimes they can be just spectators on a surface [10]. Therefore, in order to be confident in an adsorbate's contribution to the overall catalytic reaction, both steady-state and transient kinetic analysis must be performed and compared [11]. Here, the dynamic nature of the adsorbed intermediates involved in the reaction between acetone and ozone over a 10 wt. % MnO_2/SiO_2 catalyst will be discussed using the Tamaru Method.

The transient coverage versus time curves (Figs. 3.11 – 3.14) can be used to obtain adsorption and reaction rates as a function of coverage by differentiation of the data. An example of this method for the case of acetone is shown in Figure 3.15. Figure 3.15a) presents the acetone addition curve at 318 K, which shows the evolution of acetone coverage, θ_A, as a function of time when acetone is added to the reaction mixture already containing ozone. The rate of increase in coverage, $(d\theta_A/dt)_a$, is equal to the rate of acetone adsorption, r_a, minus the rate of acetone desorption, r_d, minus the rate of acetone reaction, r_{rxn}, or $(d\theta_A/dt)_a = r_a - (r_d + r_{rxn})$. Figure 3.15b) displays the acetone removal curve which shows the decay in acetone coverage, θ_A, as a function of time when acetone is removed from the reaction mixture. The rate of decrease in coverage, $-(d\theta_A/dt)_r$, is equal to the sum of the rates of acetone desorption and reaction or $-(d\theta_A/dt)_r = r_d + r_{rxn}$. As previously mentioned, the rates for acetone addition and removal were obtained by differentiating both curves with respect to time at the same coverage to obtain the slope (i.e. rate). Once the rate of acetone addition, $(d\theta_A/dt)_a$, and rate of

acetone removal, $-(d\theta_A/dt)_r$, were obtained, the rate of acetone adsorption can be calculated by the expression, $r_a = (d\theta_A/dt)_a - (d\theta_A/dt)_r$. The same procedure was followed to determine the rate of ozone adsorption using the ozone addition and removal curves.

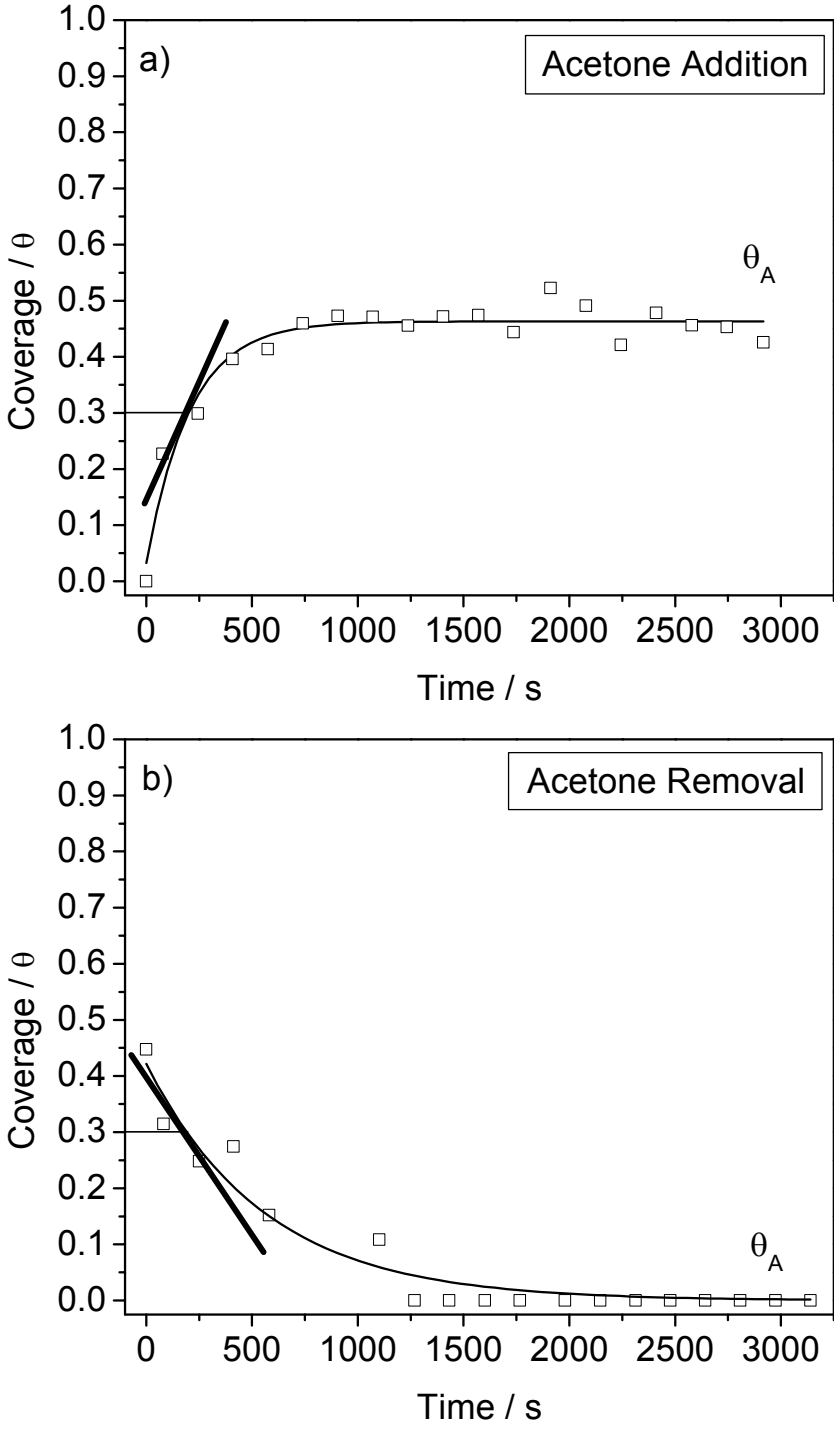

Figure 3.15. Transient kinetic analysis example for a) acetone addition and b) acetone removal.

Figure 3.16 displays the results of the transient analysis as the rate of acetone adsorption is plotted with the rate of acetone removal (Fig. 3.16a)), and the rate of ozone adsorption is plotted with the rate of ozone removal (Fig. 3.16b)). Figure 3.16a) and 3.16b) show that the rates of adsorption for both acetone and ozone adsorption decrease with increasing coverage while the rates of removal increase with increasing coverage. These are expected dependencies since the rate of adsorption is proportional to the number of empty sites and the rate of desorption to the number of occupied sites. At steady-state, the rate of adsorption is equal to the rate of removal so steady-state rate and coverage values can be obtained by the intersection of the two curves. Figure 3.16a) shows that the steady-state acetone rate was 0.00083 s^{-1}, and the steady-state coverage for the adsorbed acetone intermediate was 0.46. Figure 3.16b) shows that the steady-state ozone rate was 0.000095 s^{-1}, and the steady-state coverage for the adsorbed peroxide species was 0.087. Recall that the conditions for the addition and removal experiments utilized initial partial pressures for acetone and ozone of 193 and 793 Pa (1,900 and 7,800 ppm), respectively**,** at a temperature of 318 K. Referring to Figures 3.6 – 3.9 that displayed steady-state rates as a function of reactant partial pressure, it can be determined that the steady-state values were 0.0015 s^{-1} and 0.0086 s^{-1} for the overall rates of acetone and ozone reaction, respectively, at the conditions used in the transient experiments. Likewise, referring to Figures 3.4 and 3.5 that displayed steady-state coverages as a function of varying reactant partial pressure, the steady-state coverage values were 0.36 and 0.081 for the adsorbed acetone and ozone intermediates, respectively, at the conditions used in the transient experiments.

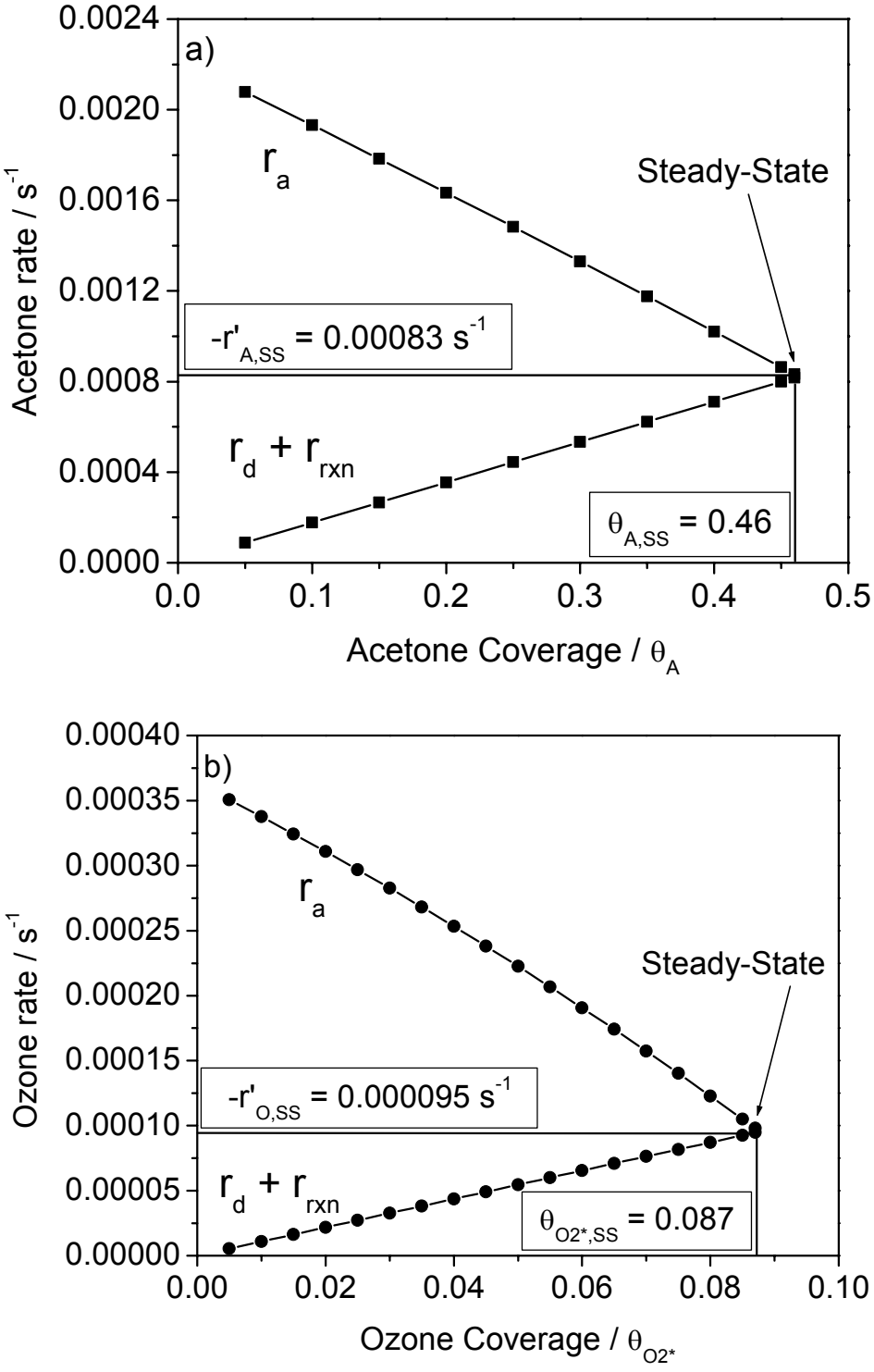

Figure 3.16. Transient kinetic analysis results to determine steady-state coverages and rates for a) acetone and b) ozone.

The steady-state rate and coverage results are compared to the rates and coverages obtained from the transient experiments in Table 3.4. As shown, the coverages obtained by the two separate techniques are in good agreement with one another. There is greater error when comparing the coverages obtained by the two techniques for the adsorbed acetone intermediate compared to the adsorbed ozone intermediate. This error is due to the small peak intensity and area attributed to the adsorbed acetone intermediate, which resulted in greater error during peak integration. When comparing the rates obtained by the two separate techniques, however, only the acetone results are in reasonable agreement. It is known from experiment, that the rates of ozone reaction are ~10 times the rates of acetone reaction. For the transient results, however, the rate of ozone reaction obtained by monitoring the adsorbed peroxide species is significantly smaller than the rate of acetone reaction obtained from monitoring the adsorbed acetone intermediate. Thus, it can be concluded the adsorbed acetone intermediate does contribute to the overall acetone oxidation reaction as described by the reaction mechanism while the adsorbed peroxide species does not contribute to the oxidation reaction. Based on this result, the main reactive species are indicated to be adsorbed atomic oxygen species as proposed in the mechanism.

Table 3.4. Steady-state and transient rate and coverage comparison.

	Steady-State Results	Transient Results
Acetone Coverage / θ_A	0.36	0.46
Peroxide Coverage / θ_{O2*}	0.081	0.087
$-r'_{A,SS}$ / s^{-1}	0.0015	0.00083
$-r'_{O,SS}$ / s^{-1}	0.0086	0.000095

3.5 Conclusions

A detailed mechanistic study of acetone oxidation using ozone was performed on a 10 wt. % silica-supported manganese oxide catalyst utilizing Raman spectroscopy, temperature programmed desorption (TPD), and kinetic measurements. *In situ* Raman spectroscopy at reaction conditions identified a band at 2930 cm^{-1} due to an adsorbed acetone species on the silica support and a band at 890 cm^{-1} due to an adsorbed peroxide species on the manganese oxide. A steady-state kinetic analysis, which varied acetone partial pressure (101 – 405 Pa), ozone partial pressure (101 – 1013 Pa), and temperature (318, 333, 343, and 373 K), was used to determine reaction rate expressions, while a transient kinetic study (318 K) was used to determine the role of the adsorbed species in the reaction mechanism. It was found that the rates of the acetone and ozone reactions were equally well described by both a power rate law and a Langmuir-Hinshelwood

expression. The transient experiments showed that the rates of formation and reaction of the observed peroxide surface species did not correspond to the overall reaction rate, and it was concluded that it was not directly involved in the rate determining step of the reaction. A mechanism is proposed involving the reaction of an adsorbed acetone intermediate with an atomically adsorbed oxygen species via a dual site surface reaction to form complete oxidation products.

References

1 R. M. Felder, R. W. Rousseau, "Elementary Principles of Chemical Processes, Second Ed.," John Wiley & Sons: New York, 1986, 235.

2 W. Li, S. T. Oyama, Mechanism of ozone decomposition on a manganese oxide catalyst. 1. In situ Raman spectroscopy and ab initio molecular orbital calculations, *J. Am. Chem. Soc*., **1998**, 120, 9041.

3 W. Li, S. T. Oyama, Mechanism of ozone decomposition on a mangense oxide catalyst. 2. Steady-state and transient kinetic studies, *J. Am. Chem. Soc.*, **1998**, 120, 9047.

4 Copyright © 2005, Mordechai Shacham, Michael B. Cutlip and Michael Elly.

5 W. S. Sim, D. A. King, Mechanism of acetone oxidation on Ag{111}-p(4 × 4)-O, *J. Phys. Chem*., **1996**, 100, 14794.

6 M. L. Sauer, D. F. Ollis, Acetone oxidation in a photocatalytic monolith reactor, *J. Catal*., **1994**, 149, 81.

7 G. I. Golodets, V. V. Borovik, V. M Vorotyntsev, Mechanism and kinetics of the selective catalytic oxidation of acetone, *Teor. Eksp. Khim*., **1986**, 22, 252.

8 NIST Chemistry WebBook, "http://webbook.nist.gov/", 6, April, 2005.

9 K. Tamaru, "Dynamic Heterogeneous Catalysis," Academic Press: London, 1978.

10 W. Zhang, S. T. Oyama, In situ laser Raman studies of intermediates in the catalytic oxidation of ethanol over supported molybdenum oxide, *J. Phys. Chem*., **1996**, 100, 10759.

11 S. T. Oyama, W. Li, Absolute determination of reaction mechanisms by in situ measurements of reaction intermediates, *Top. Catal*., **1999**, 8, 75.